Received: 17 November 2023 | Accepted: 26 August 2024

DOI: 10.1002/rnc.7643

RESEARCH ARTICLE

WILEY

Robust internal model-based control for linear-time-invariant systems

Atabak Azimi | **Stefan Koch** | **Markus Reichhartinger**

Institute of Automation and Control, Graz University of Technology, Graz, Austria

Correspondence
Atabak Azimi, Institute of Automation and Control, Graz University of Technology, Graz, Austria.
Email: atabak.azimi@tugraz.at

[Correction added on 25 September 2024, after first online publication: the ORCID ID of Atabak Azimi and Markus Reichhartinger have been added.]

Abstract

This article addresses robust output regulation for systems affected by disturbances generated by an uncertain exosystem as well as matched external disturbances. The robustness of the feedback loop is achieved by combining internal model based control with sliding mode control, resulting in a structurally simple controller. The design of the proposed controller is presented first for the full information problem, that is, the disturbances generated by the exosystem and the state-information is available for the control algorithm. This requirement is relaxed in the second step of the controller design, where the observer-based robust output feedback-loop structure is developed. Results from a comparative simulation study are presented to illustrate the advantages and the effectiveness of the proposed controller concept.

KEYWORDS

internal-model based control, model uncertainties, robust control, sliding mode control, time-varying disturbance

1 | INTRODUCTION

Periodic disturbances are common perturbations which numerous real plants encounter.[1–3] The "Internal Model Principle" or "Internal model-based control" (IMC) is one of the prominent tools for dealing with such disturbances in linear[4] and nonlinear systems.[5] Controllers based on the IMC principle are known to be robust against external disturbances that are generated by an exogenous system (exosystem), including combinations of harmonic functions with different frequencies and polynomials in time. Exploiting a model of the exosystem in the controller, IMC produces a disturbance related signal and injects it into the plant to compensate for the actual disturbance's effect. In this manner, exact disturbance rejection is achieved.

Although this methodology performs precisely in the case of complete knowledge of the exosystem, it faces difficulties dealing with uncertain situations. For instance, when the frequency is unknown, a nondecaying bounded system output may be observed even when the frequency is constant. In order to deal with this issue, some works[6–10] suggest adaptive IMC. The idea is that an extra part is added to the controller for searching the proper frequency that is then used in the IMC.[6] Besides the excellent performance of adaptive IMC in dealing with uncertainties in the model of the exosystem, it also renders the controller more complex. In particular, the adaptive and the IMC parts are assumed to be captured by a slow and a fast dynamics respectively .[11] Hence, proper tuning of the entire feedback loop, requires information on the

disturbance which makes the tuning of the adaptive part challenging. The adaptive IMC is also promising for time-varying frequencies in the disturbance, [12] but the above mentioned challenges are still open for practical cases.

Recent advancements in control methodologies have increasingly integrated IMC into sliding mode control (SMC) to enhance robustness and precision across various applications. There are two categories which can be distinguished: model-free[13] and model-based.[14] In model-free sliding mode control, the entire system and disturbances are treated as uncertainties. This approach is particularly advantageous for systems where developing an accurate model is time-consuming and computationally expensive.[15] On the other hand, in model-based sliding mode control, the system model and disturbances are explicitly accounted for in the control design. This approach leverages the available model information to achieve a narrower band for the uncertainty, making it particularly effective for systems where modeling is feasible and beneficial. The model-based version of SMC has been used to combine with IMC in various applications. For instance, a robust IMC-SMC hybrid approach has been proposed in Reference 16 to improve the robustness of servo motor control systems. The therein presented method leverages the robustness of SMC to handle model uncertainties and disturbances while maintaining the benefits of IMC for disturbance rejection and precise control. The authors demonstrated through simulations and experiments that their approach significantly outperforms traditional control methods regarding disturbance rejection and tracking accuracy.

Similarly, the integration of IMC into SMC for high-precision electro-optical tracking systems has been investigated in Reference 17. The focus was on addressing the challenges of high-frequency disturbances and model uncertainties inherent in such systems. Their results showed enhanced control precision and robustness, validating the effectiveness of combining IMC with SMC in practical applications.

Furthermore a combination between IMC and SMC with the idea of separating a matched disturbance into a modeled and a remaining unknown part has been proposed in Reference 18. This approach is similar to the techniques summarized in Reference 19 and the therein given references, where also a matched disturbance is assumed to be composed of a structured and a remaining unstructured part. All of the mentioned approaches assume a matched disturbance consisting of a modeled or structured and a remaining un-modeled part. In all cases, the latter one is compensated by some sliding mode based action within the control signal. Compared to adaptive IMC, the resulting controllers bring less complexity into the design process while maintaining the beneficial properties of the adaptive approach.

In contrast to the above cited papers, in this article, the model of the exosystem is allowed to be uncertain, and, additionally, its generated disturbances are not necessarily matched. This yields a fundamentally different approach. Besides, a matched uncertainty is also taken into account in the design of the proposed control law. Consequently, the aforementioned approaches[18,19] can also be applied. The main theoretical contributions of this article are summarized as follows:

- The model of the exosystem is allowed to be uncertain. This systematically broadens the class of admissible disturbances to include harmonic signals with unknown and even time-varying frequencies.
- Generated disturbances that are not necessarily matched are handled by the proposed control law, providing a more robust solution compared to existing methods.
- A matched external uncertainty also is integrated into the proposed method, ensuring compatibility with existing approaches.
- An output feedback generalization of the controller is developed, representing a novel aspect of the presented methodology.

Although the proposed algorithms are not limited to first-order sliding mode controllers in principle, this work focuses on this type without further exploiting higher-order sliding mode controllers.

The article is structured as follows: In the next section the problem formulation is described and in Section 3, the controller design for two cases is presented. The case of available state and disturbance information for feedback and the observer case are investigated in Section 3. Section 4 provides a simulation example of a plant, where IMC, SMC, adaptive IMC and internal model-based sliding mode control (IMSMC) are implemented for three scenarios and their performance is compared. Finally, the pinpoint of the article and future research directions are highlighted in Section 5.

2 | PROBLEM FORMULATION

In this article a disturbed nth order plant model given by the linear time-invariant system

$$\dot{\mathbf{x}} = \mathbf{A}\mathbf{x} + \mathbf{b}(u + \delta(t)) + \mathbf{P}\mathbf{w}, \tag{1a}$$

$$y = \mathbf{c}^{\mathrm{T}}\mathbf{x}, \tag{1b}$$

with the state vector $\mathbf{x} \in \mathbb{R}^n$, the control input $u \in \mathbb{R}$, and the system output $y \in \mathbb{R}$ is considered. The disturbance has two parts: a structured part, denoted by $\mathbf{w} \in \mathbb{R}^p$, and an unstructured part, denoted by $\delta \in \mathbb{R}$. The $n \times n$ dynamic matrix of system (1) is denoted by $\mathbf{A}$ and the $n \times p$ input matrix $\mathbf{P}$ takes into account the impact of the disturbance $\mathbf{w}$. Furthermore, the $n \times 1$ vector $\mathbf{b}$ represents the effect of the control input u in the dynamics of system (1), and the $n \times 1$ vector $\mathbf{c}$ demonstrate the influence of the state $\mathbf{x}$ in the output y of the system (1). The unstructured disturbance, $\delta(t)$, is applied to the same channel as the control input, and its magnitude is assumed to be bounded, that is, $|\delta(t)| < \Delta_\delta$. The structured disturbance is generated by the so-called exosystem

$$\dot{\mathbf{w}} = (\mathbf{S}_{\mathrm{n}} + \mathbf{S}_\Delta(t))\mathbf{w} = \mathbf{S}\mathbf{w}. \tag{2}$$

The matrix $\mathbf{S} \in \mathbb{R}^{p\times p}$ is the dynamic matrix of the exosystem (2). The constant matrix $\mathbf{S}_{\mathrm{n}}$ is known, whereas the matrix $\mathbf{S}_\Delta$ is unknown and therefore introduces the uncertainty in the exosystem.

Assumption 1. All eigenvalues of the real matrices $\mathbf{S}$ and $\mathbf{S}_{\mathrm{n}}$ have zero real part for all time t.

Remark 1. The matrix $\mathbf{S}_\Delta(t)$ allows to have time-varying elements representing uncertainties in the frequencies of the periodic disturbances. Besides generating the disturbance $\mathbf{w}$, the exosystem also can be exploited to generate a scalar reference signal $-\mathbf{q}^{\mathrm{T}}\mathbf{w}$ with $\mathbf{q} \in \mathbb{R}^p$, which is, due to Assumption 1, a periodic or constant function of time.

The problem tackled in this article is the design of a robust output feedback controller for system (1a) which drives the system output y to the reference $-\mathbf{q}^{\mathrm{T}}\mathbf{w}$. Defining the scalar output $\sigma = y + \mathbf{q}^{\mathrm{T}}\mathbf{w}$ for system (1a), that is,

$$\dot{\mathbf{x}} = \mathbf{A}\mathbf{x} + \mathbf{b}(u + \delta(t)) + \mathbf{P}\mathbf{w}, \tag{3a}$$

$$\sigma = \mathbf{c}^{\mathrm{T}}\mathbf{x} + \mathbf{q}^{\mathrm{T}}\mathbf{w}, \tag{3b}$$

the goal is to make σ vanish in steady state. Thus,

$$\lim_{t\to\infty} \sigma(t) = 0, \tag{4}$$

should hold despite the uncertainty introduced by $\mathbf{S}_\Delta$ and the disturbance $\delta(t)$.

Assumption 2. The pair $(\mathbf{A}, \mathbf{b})$ is stabilizable and the pair $(\mathbf{A}, \mathbf{c})$ is observable.

This is a well-known assumption for the existence of an output feedback controller.[6]

3 | CONTROLLER DESIGN

The control algorithm proposed in this article is developed and presented step by step. First, the so-called full information problem is investigated. Therein, the state vector $\mathbf{x}$ and the disturbance $\mathbf{w}$ are assumed to be available for feedback, see Section 3.1. This assumption is relaxed in Section 3.2 where an observer is introduced for solving the output feedback problem.

3.1 | Full knowledge on state and disturbance

In order to design controllers counteracting against the impact of the structured disturbance $\mathbf{w}$ in steady state, and therefore satisfying (4), IMC is a powerful method.[6] Therein, the control input

$$u = -\mathbf{k}^{\mathrm{T}}\mathbf{x} + \mathbf{l}^{\mathrm{T}}\mathbf{w}, \tag{5}$$

where the $n \times 1$ vector $\mathbf{k}$ is designed to place the eigenvalues of $\mathbf{A} - \mathbf{b}\mathbf{k}^{\mathrm{T}}$ at desired locations to achieve asymptotic stability of the closed-loop system. The second part in (5) manages the structured disturbance rejection and reference tracking problem in absence of δ. In the design process of IMC the $p \times 1$ vector $\mathbf{l}$ is computed using $\mathbf{S}_{\mathrm{n}}$ only. In this nominal case it is shown[5] that the state vector $\mathbf{x}$ converges towards the steady state

$$\mathbf{x}_{\infty} = \mathbf{\Pi}\mathbf{w}, \tag{6}$$

and σ goes to zero. In (6) the $n \times p$ matrix $\mathbf{\Pi}$ as well as the vector $\mathbf{l}$ in (5) are computed such that the equations

$$\mathbf{\Pi}\mathbf{S}_{\mathrm{n}} = (\mathbf{A} - \mathbf{b}\mathbf{k}^{\mathrm{T}})\mathbf{\Pi} + \mathbf{b}\mathbf{l}^{\mathrm{T}} + \mathbf{P}, \tag{7a}$$

$$0 = \mathbf{c}^{\mathrm{T}}\mathbf{\Pi} + \mathbf{q}^{\mathrm{T}}, \tag{7b}$$

hold. This set of equations is obtained by inserting (6) into (3a) and (3b) and using (2). Furthermore, the existence of the steady state solution $\mathbf{x}_{\infty}$ is ensured by tuning $\mathbf{k}$ such that $(\mathbf{A} - \mathbf{b}\mathbf{k}^{\mathrm{T}})$ is a Hurwitz matrix. Note that a unique solution for $\mathbf{\Pi}$ and $\mathbf{l}$ is guaranteed by Lemma 1.4.2 in Reference 6. Consequently, this approach solves the considered problem in the nominal case, that is, $\mathbf{S}_{\Delta} = \mathbf{0}$ and $\delta(t) = 0$. However, it is not robust against the perturbation characterized by $\mathbf{S}_{\Delta} \neq \mathbf{0}$ and $\delta(t) \neq 0$. Therein, equation (6) will not be satisfied and, as a result, the deviation

$$\tilde{\mathbf{x}} = \mathbf{x} - \mathbf{\Pi}\mathbf{w} \tag{8}$$

will not vanish. In this scenario and in the case $\delta = 0$, instead of having a vanishing output σ, a bounded and non-vanishing response can be observed. In contrast to the adaptive IMC methods proposed in References 20–22, in this article a sliding mode based approach is presented. It relies on an additive extension of the control input in (5), that is,

$$u = -\mathbf{k}^{\mathrm{T}}\mathbf{x} + \mathbf{l}^{\mathrm{T}}\mathbf{w} + u_{\mathrm{s}}. \tag{9}$$

The proper choice of the new control action u_{s} is presented in Theorem 1. Lemma 1, which is stated below, is a prerequisite for the proof of Theorem 1.

Lemma 1. *The elements of the state vector* $\mathbf{x}$ *of the system*

$$\dot{\mathbf{x}} = \left(\mathbf{I}_n - \frac{\mathbf{b}\mathbf{c}^{\mathrm{T}}}{\mathbf{c}^{\mathrm{T}}\mathbf{b}}\right)\mathbf{A}\mathbf{x} + \mathbf{B}\mathbf{w}, \tag{10}$$

$$\sigma = \mathbf{c}^{\mathrm{T}}\mathbf{x} + \mathbf{q}^{\mathrm{T}}\mathbf{w}, \tag{11}$$

remain bounded as long as the system $(\mathbf{A}, \mathbf{b}, \mathbf{c}^{\mathrm{T}})$ *is minimum phase,* $\mathbf{w}$ *is bounded and* σ *is zero after finite time. The proof is in Appendix A.*

Theorem 1. *Given plant (3) and assume a constant relative degree one from output* σ *to input* u*. Let the disturbance* $\mathbf{w}$ *be generated by the uncertain exosystem (2). Then the control input* u *from equation (9) with*

$$u_{\mathrm{s}} = -\tfrac{1}{\mathbf{c}^{\mathrm{T}}\mathbf{b}}\left[\mathbf{c}^{\mathrm{T}}\left(\mathbf{A} - \mathbf{b}\mathbf{k}^{\mathrm{T}}\right)(\mathbf{x} - \mathbf{\Pi}\mathbf{w}) + k_{\mathrm{s}}\mathrm{sign}(\sigma) + k_{\lambda}\sigma\right] \tag{12}$$

ensures that the output σ vanishes in finite time as long as the vectors $\mathbf{k}$ and $\mathbf{l}$ are selected such that $\mathbf{A}-\mathbf{b}\mathbf{k}^{\mathrm{T}}$ is a Hurwitz matrix and the regulator equations (7) is satisfied, the positive constants k_λ and k_s are selected such that

$$k_\lambda \geq 0 \quad \text{and} \quad k_s > \sup_t \left|\mathbf{q}^{\mathrm{T}}\mathbf{S}_\Delta(t)\mathbf{w}(t) + \mathbf{c}^{\mathrm{T}}\mathbf{b}\delta(t)\right|, \tag{13}$$

and $\mathbf{q}^{\mathrm{T}}\mathbf{S}_\Delta(t)\mathbf{w}(t)$ is bounded. Furthermore, if the transfer function from u to σ is minimum phase, the internal dynamics are input-to-state stable.

Proof of Theorem 1: First the case $k_\lambda = 0$ is investigated. For disturbance rejection, $\sigma = 0$ is considered as sliding surface. The first time derivative of σ considering (7) yields

$$\begin{aligned}\dot{\sigma} &= \mathbf{c}^{\mathrm{T}}\left((\mathbf{A}-\mathbf{b}\mathbf{k}^{\mathrm{T}})\mathbf{x} + (\mathbf{b}\mathbf{l}^{\mathrm{T}}+\mathbf{P})\mathbf{w} + \mathbf{b}\delta + \mathbf{b}u_s\right) + \mathbf{q}^{\mathrm{T}}\mathbf{S}\mathbf{w} = \\ &= \mathbf{c}^{\mathrm{T}}\left((\mathbf{A}-\mathbf{b}\mathbf{k}^{\mathrm{T}})(\tilde{\mathbf{x}}+\mathbf{\Pi}\mathbf{w}) + (\mathbf{b}\mathbf{l}^{\mathrm{T}}+\mathbf{P})\mathbf{w}\right) + \mathbf{q}^{\mathrm{T}}\mathbf{S}\mathbf{w} + \mathbf{c}^{\mathrm{T}}\mathbf{b}\delta + \mathbf{c}^{\mathrm{T}}\mathbf{b}u_s = \\ &= \mathbf{q}^{\mathrm{T}}\mathbf{S}_\Delta\mathbf{w} + \mathbf{c}^{\mathrm{T}}\mathbf{b}\delta - k_s\mathrm{sign}(\sigma).\end{aligned} \tag{14}$$

Defining the scalar

$$\Delta(\mathbf{w}(t), t) = \mathbf{q}^{\mathrm{T}}\mathbf{S}_\Delta(t)\mathbf{w}(t) + \mathbf{c}^{\mathrm{T}}\mathbf{b}\delta(t) \tag{15}$$

equation (14) can be written as

$$\dot{\sigma} = \Delta - k_s\mathrm{sign}(\sigma). \tag{16}$$

Considering the selection of k_s from equation (13) ensures that $\eta(\mathbf{w}(t), t) = k_s - \Delta > 0$. Selecting the minimum value of η as $\eta_{\min}$, two situations can occur: $\sigma > 0$ and $\sigma < 0$. The first time derivative of σ for both situations and the expression $\sigma\dot{\sigma}$ are

$$\begin{cases} \dot{\sigma} = \Delta - k_s \leq -\eta_{\min}, & \sigma\dot{\sigma} < -\eta_{\min}|\sigma| \qquad \sigma > 0, \\ \dot{\sigma} = \Delta + k_s \geq \eta_{\min}, & \sigma\dot{\sigma} < -\eta_{\min}|\sigma| \qquad \sigma < 0. \end{cases} \tag{17}$$

In both cases $\sigma\dot{\sigma} < -\eta_{\min}|\sigma|$ and, based on the η-reachability condition,[23,24] σ converges to zero in finite time, and the reaching time t_r follows $t_r \leq \frac{|\sigma(0)|}{\eta_{\min}}$.

Now the closed-loop stability is investigated. The control input is rearranged in a more suitable way as

$$u = -\left(\mathbf{k}^{\mathrm{T}} + \tfrac{\mathbf{c}^{\mathrm{T}}(\mathbf{A}-\mathbf{b}\mathbf{k}^{\mathrm{T}})}{\mathbf{c}^{\mathrm{T}}\mathbf{b}}\right)\mathbf{x} + \left(\mathbf{l}^{\mathrm{T}} + \tfrac{\mathbf{c}^{\mathrm{T}}(\mathbf{A}-\mathbf{b}\mathbf{k}^{\mathrm{T}})\mathbf{\Pi}}{\mathbf{c}^{\mathrm{T}}\mathbf{b}}\right)\mathbf{w} - \frac{k_s\mathrm{sign}(\sigma)}{\mathbf{c}^{\mathrm{T}}\mathbf{b}}. \tag{18}$$

The closed loop system consisting of plant (3a) and the controller as written in (18) is governed by

$$\dot{\mathbf{x}} = \left((\mathbf{A}-\mathbf{b}\mathbf{k}^{\mathrm{T}}) - \frac{\mathbf{b}\mathbf{c}^{\mathrm{T}}(\mathbf{A}-\mathbf{b}\mathbf{k}^{\mathrm{T}})}{\mathbf{c}^{\mathrm{T}}\mathbf{b}}\right)\mathbf{x} + \left(\mathbf{P} + \mathbf{b}\mathbf{l}^{\mathrm{T}} + \frac{\mathbf{b}\mathbf{c}^{\mathrm{T}}(\mathbf{A}-\mathbf{b}\mathbf{k}^{\mathrm{T}})\mathbf{\Pi}}{\mathbf{c}^{\mathrm{T}}\mathbf{b}}\right)\mathbf{w} + \mathbf{b}\delta - \mathbf{b}\frac{k_s\mathrm{sign}(\sigma)}{\mathbf{c}^{\mathrm{T}}\mathbf{b}}. \tag{19}$$

The dynamic matrix in (19) can be simplified as

$$(\mathbf{A}-\mathbf{b}\mathbf{k}^{\mathrm{T}}) - \frac{\mathbf{b}\mathbf{c}^{\mathrm{T}}(\mathbf{A}-\mathbf{b}\mathbf{k}^{\mathrm{T}})}{\mathbf{c}^{\mathrm{T}}\mathbf{b}} = \left(\mathbf{I}_n - \frac{\mathbf{b}\mathbf{c}^{\mathrm{T}}}{\mathbf{c}^{\mathrm{T}}\mathbf{b}}\right)(\mathbf{A}-\mathbf{b}\mathbf{k}^{\mathrm{T}}) = \left(\mathbf{I}_n - \frac{\mathbf{b}\mathbf{c}^{\mathrm{T}}}{\mathbf{c}^{\mathrm{T}}\mathbf{b}}\right)\mathbf{A}, \tag{20}$$

where it is worth to note that multiplying $\left(\mathbf{I}_n - \frac{\mathbf{b}\mathbf{c}^{\mathrm{T}}}{\mathbf{c}^{\mathrm{T}}\mathbf{b}}\right)$ with $\mathbf{b}\mathbf{k}^{\mathrm{T}}$ from the right side creates a zero matrix. Hence, the choice of $\mathbf{k}$ does not affect the closed loop dynamic matrix in (19) which, using the above developed results, can be written as

$$\dot{\mathbf{x}} = \left(\mathbf{I}_n - \tfrac{\mathbf{b}\mathbf{c}^{\mathrm{T}}}{\mathbf{c}^{\mathrm{T}}\mathbf{b}}\right)\mathbf{A}\mathbf{x} + \left(\mathbf{P} + \mathbf{b}\mathbf{l}^{\mathrm{T}} + \tfrac{\mathbf{b}\mathbf{c}^{\mathrm{T}}(\mathbf{A}-\mathbf{b}\mathbf{k}^{\mathrm{T}})\mathbf{\Pi}}{\mathbf{c}^{\mathrm{T}}\mathbf{b}}\right)\mathbf{w} - \mathbf{b}\frac{k_s\mathrm{sign}(\sigma)}{\mathbf{c}^{\mathrm{T}}\mathbf{b}} + \mathbf{b}\delta. \tag{21}$$

In order to determine the eigenvalues of the closed-loop dynamic matrix in (21), its characteristic polynomial is computed, that is,

$$\begin{aligned}\det\left[s\mathbf{I}_n-\left(\mathbf{I}_n-\frac{\mathbf{b}\mathbf{c}^{\mathrm{T}}}{\mathbf{c}^{\mathrm{T}}\mathbf{b}}\right)\mathbf{A}\right]&=\det\left[\left(\mathbf{I}_n+\frac{\mathbf{b}\mathbf{c}^{\mathrm{T}}\mathbf{A}}{\mathbf{c}^{\mathrm{T}}\mathbf{b}}(s\mathbf{I}_n-\mathbf{A})^{-1}\right)(s\mathbf{I}_n-\mathbf{A})\right]=\\&=\det(s\mathbf{I}_n-\mathbf{A})\left(1+\frac{\mathbf{c}^{\mathrm{T}}\mathbf{A}(s\mathbf{I}_n-\mathbf{A})^{-1}\mathbf{b}}{\mathbf{c}^{\mathrm{T}}\mathbf{b}}\right)=\det(s\mathbf{I}_n-\mathbf{A})\frac{sG(s)}{\mathbf{c}^{\mathrm{T}}\mathbf{b}},\end{aligned}\tag{22}$$

where

$$\det(\mathbf{I}_n+\mathbf{u}\mathbf{v}^{\mathrm{T}})=1+\mathbf{v}^{\mathrm{T}}\mathbf{u}\tag{23}$$

for some vectors $\mathbf{v}$ and $\mathbf{u}$ of appropriate dimensions was used. In (22), the complex variable s appears due to the Laplace transform and $\mathbf{I}_n$ is the identity matrix of order n. The transfer function $G(s)$ from control input u to output σ of plant (3) further can be expressed as

$$G(s)=\mathbf{c}^{\mathrm{T}}(s\mathbf{I}_n-\mathbf{A})^{-1}\mathbf{b}=\frac{\mu(s)}{\det(s\mathbf{I}_n-\mathbf{A})},\tag{24}$$

where $\mu(s)$ denotes the numerator polynomial of G. This allows to rewrite equation (22) as

$$\det(s\mathbf{I}_n-\mathbf{A})\frac{sG(s)}{\mathbf{c}^{\mathrm{T}}\mathbf{b}}=\frac{s\mu(s)}{\mathbf{c}^{\mathrm{T}}\mathbf{b}}.\tag{25}$$

As a result, the eigenvalues of the closed loop dynamic matrix in (21) are the combination of 0 and the roots of the polynomial $\mu(s)$. The latter one, corresponding to the internal dynamics, are the $n-1$ zeros of the plant (3) with the relative degree one output σ. The transfer function from input u to the output σ of the system (3) is minimum phase by assumption and consequently $\mu(s)$ is a Hurwitz polynomial and the internal dynamics are input to state stable.[25] Hence, in the case of a bounded input, boundedness of the state vector $\mathbf{x}$ of system (21) is ensured by applying Lemma 1.

In the general case, that is, $k_\lambda\neq 0$, the sliding variable remains the same as in the special case, that is, the output σ. The dynamics of the sliding variable is similar to (14); however, it contains the additional term $k_\lambda\sigma$, that is,

$$\dot{\sigma}=\mathbf{q}^{\mathrm{T}}\mathbf{S}_\Delta\mathbf{w}+\mathbf{c}^{\mathrm{T}}\mathbf{b}\delta-k_{\mathrm{s}}\mathrm{sign}(\sigma)-k_\lambda\sigma.\tag{26}$$

Defining Δ as in (15), the final form of the dynamics of the sliding variable is

$$\dot{\sigma}=\Delta-k_{\mathrm{s}}\mathrm{sign}(\sigma)-k_\lambda\sigma.\tag{27}$$

Equation (27) has the similar form as a constant plus proportional reaching law[24] and the controller rejects the disturbance and force the output σ to zero. For closed-loop stability and boundedness, the controller is rewritten as

$$u=-\mathbf{k}^{\mathrm{T}}\mathbf{x}+\mathbf{l}^{\mathrm{T}}\mathbf{w}-\tfrac{1}{\mathbf{c}^{\mathrm{T}}\mathbf{b}}\left(\mathbf{c}^{\mathrm{T}}(\mathbf{A}-\mathbf{b}\mathbf{k}^{\mathrm{T}})(\mathbf{x}-\mathbf{\Pi}\mathbf{w})+k_{\mathrm{s}}\mathrm{sign}(\sigma)+k_\lambda\sigma\right).\tag{28}$$

The closed-loop of the system (3a) with input controller (28) is in the form

$$\begin{aligned}\dot{\mathbf{x}}&=\left(\mathbf{I}_n-\frac{\mathbf{b}\mathbf{c}^{\mathrm{T}}}{\mathbf{c}^{\mathrm{T}}\mathbf{b}}\right)\mathbf{A}\mathbf{x}+\left(\mathbf{P}+\mathbf{b}\mathbf{l}^{\mathrm{T}}+\frac{\mathbf{b}\mathbf{c}^{\mathrm{T}}(\mathbf{A}-\mathbf{b}\mathbf{k}^{\mathrm{T}})\mathbf{\Pi}}{\mathbf{c}^{\mathrm{T}}\mathbf{b}}\right)\mathbf{w}+\mathbf{b}\delta-\mathbf{b}\frac{k_{\mathrm{s}}\mathrm{sign}(\sigma)}{\mathbf{c}^{\mathrm{T}}\mathbf{b}}-\mathbf{b}\frac{k_\lambda\sigma}{\mathbf{c}^{\mathrm{T}}\mathbf{b}}=\\&=\left(\mathbf{A}-\frac{\mathbf{b}\mathbf{c}^{\mathrm{T}}}{\mathbf{c}^{\mathrm{T}}\mathbf{b}}\mathbf{A}-\frac{\mathbf{b}\mathbf{c}^{\mathrm{T}}}{\mathbf{c}^{\mathrm{T}}\mathbf{b}}k_\lambda\right)\mathbf{x}+\left(\mathbf{P}+\mathbf{b}\mathbf{l}^{\mathrm{T}}+\frac{\mathbf{b}\mathbf{c}^{\mathrm{T}}(\mathbf{A}-\mathbf{b}\mathbf{k}^{\mathrm{T}})\mathbf{\Pi}}{\mathbf{c}^{\mathrm{T}}\mathbf{b}}-\frac{\mathbf{b}\mathbf{q}^{\mathrm{T}}}{\mathbf{c}^{\mathrm{T}}\mathbf{b}}k_\lambda\right)\mathbf{w}+\mathbf{b}\delta-\mathbf{b}\frac{k_{\mathrm{s}}\mathrm{sign}(\sigma)}{\mathbf{c}^{\mathrm{T}}\mathbf{b}}.\end{aligned}\tag{29}$$

Similar to (22), the eigenvalues of the dynamic matrix in (29) are computed as

$$\det\left[s\mathbf{I}_n-\left(\mathbf{A}-\frac{\mathbf{b}\mathbf{c}^{\mathrm{T}}}{\mathbf{c}^{\mathrm{T}}\mathbf{b}}\mathbf{A}-\frac{\mathbf{b}\mathbf{c}^{\mathrm{T}}}{\mathbf{c}^{\mathrm{T}}\mathbf{b}}k_\lambda\right)\right]=\det\left[\left(\mathbf{I}_n+\frac{\mathbf{b}\mathbf{c}^{\mathrm{T}}(\mathbf{A}+k_\lambda\mathbf{I}_n)}{\mathbf{c}^{\mathrm{T}}\mathbf{b}}(s\mathbf{I}_n-\mathbf{A})^{-1}\right)(s\mathbf{I}_n-\mathbf{A})\right]= \\ =\det(s\mathbf{I}_n-\mathbf{A})\frac{(s+k_\lambda)G(s)}{\mathbf{c}^{\mathrm{T}}\mathbf{b}}=\frac{(s+k_\lambda)\mu(s)}{\mathbf{c}^{\mathrm{T}}\mathbf{b}}. \tag{30}$$

Hence, the set of eigenvalues are $-k_\lambda$ and the $n-1$ zeros of the plant (3). Since the system is minimum phase, $k_\lambda>0$, and the other inputs in (29) are bounded, the closed-loop is stable. □

Remark 2. Note that $k_\lambda\neq 0$ shifts the zero eigenvalue to $-k_\lambda$ and consequently produces an asymptotically stable dynamic matrix in system (30). Furthermore, it is known that this constant plus proportional reaching law impacts the dynamics during the reaching phase.[24]

3.2 | Observer case

In this section, the observer case where only σ is available, is investigated. Based on Assumption 2, system (3) is observable. Then to estimate the state $\mathbf{x}$ and the disturbance $\mathbf{w}$, a Luenberger observer is designed .[26] The structure of this observer with system (3a) is

$$\begin{aligned}\dot{\hat{\mathbf{x}}}&=\mathbf{A}\hat{\mathbf{x}}+\mathbf{P}\hat{\mathbf{w}}+\mathbf{b}u+\mathbf{g}_1(\sigma-\hat{\sigma}),\\ \dot{\hat{\mathbf{w}}}&=\mathbf{S}_{\mathrm{n}}\hat{\mathbf{w}}+\mathbf{g}_2(\sigma-\hat{\sigma}),\\ \hat{\sigma}&=\mathbf{c}^{\mathrm{T}}\hat{\mathbf{x}}+\mathbf{q}^{\mathrm{T}}\hat{\mathbf{w}},\end{aligned} \tag{31}$$

where $\hat{\mathbf{x}}$, $\hat{\mathbf{w}}$, and $\hat{\sigma}$ are estimated state, disturbance and output, and $\mathbf{g}_1\in\mathbb{R}^{n\times 1}$, $\mathbf{g}_2\in\mathbb{R}^{p\times 1}$ are the observer gains respectively. This observer also can be represented in the matrix-vector form

$$\begin{bmatrix}\dot{\hat{\mathbf{x}}}\\ \dot{\hat{\mathbf{w}}}\end{bmatrix}=\left(\begin{bmatrix}\mathbf{A}&\mathbf{P}\\ \mathbf{0}&\mathbf{S}_{\mathrm{n}}\end{bmatrix}-\begin{bmatrix}\mathbf{g}_1\\ \mathbf{g}_2\end{bmatrix}\begin{bmatrix}\mathbf{c}^{\mathrm{T}}&\mathbf{q}^{\mathrm{T}}\end{bmatrix}\right)\begin{bmatrix}\hat{\mathbf{x}}\\ \hat{\mathbf{w}}\end{bmatrix}+\begin{bmatrix}\mathbf{b}\\ \mathbf{0}\end{bmatrix}u+\begin{bmatrix}\mathbf{g}_1\\ \mathbf{g}_2\end{bmatrix}\sigma, \tag{32}$$

Theorem 2. *Given plant (3) with all assumptions from Theorem 1 and the disturbance from (2), the controller*

$$u=-\mathbf{k}^{\mathrm{T}}\hat{\mathbf{x}}+\mathbf{l}^{\mathrm{T}}\hat{\mathbf{w}}-\frac{1}{\mathbf{c}^{\mathrm{T}}\mathbf{b}}\left[\mathbf{c}^{\mathrm{T}}(\mathbf{A}-\mathbf{b}\mathbf{k}^{\mathrm{T}})(\hat{\mathbf{x}}-\mathbf{\Pi}\hat{\mathbf{w}})+k_{\mathrm{s}}\mathrm{sign}(\sigma)+k_\lambda\sigma\right] \tag{33}$$

ensures that the output σ vanishes exponentially. In equation (33), $\mathbf{l}$ and $\mathbf{\Pi}$ are the solution of the regulator equations (7). Besides, $\hat{\mathbf{x}}$ and $\hat{\mathbf{w}}$ are computed from the Luenberger observer (31) and

$$k_\lambda\geq 0\quad,\quad k_{\mathrm{s}}>\Delta_{Max}\geq|\Delta_{\mathrm{obsv}}|, \tag{34}$$

$$\Delta_{\mathrm{obsv}}=\mathbf{q}^{\mathrm{T}}\mathbf{S}_\Delta\mathbf{w}+\left(\mathbf{c}^{\mathrm{T}}\mathbf{b}\mathbf{k}^{\mathrm{T}}+\mathbf{c}^{\mathrm{T}}(\mathbf{A}-\mathbf{b}\mathbf{k}^{\mathrm{T}})\right)\mathbf{e}_{\mathbf{x}}-\left(\mathbf{c}^{\mathrm{T}}\mathbf{b}\mathbf{l}^{\mathrm{T}}+\mathbf{c}^{\mathrm{T}}(\mathbf{A}-\mathbf{b}\mathbf{k}^{\mathrm{T}})\mathbf{\Pi}\right)\mathbf{e}_{\mathbf{w}}+\mathbf{c}^{\mathrm{T}}\mathbf{b}\delta, \tag{35}$$

where

$$\mathbf{e}_{\mathbf{x}}=\mathbf{x}-\hat{\mathbf{x}}\quad,\quad\mathbf{e}_{\mathbf{w}}=\mathbf{w}-\hat{\mathbf{w}}, \tag{36}$$

are estimation errors.

Remark 3. Pushing the eigenvalues of the observer system (31) more in the left-hand side of the imaginary axis, the estimation errors $\mathbf{e}_{\mathbf{x}}$ and $\mathbf{e}_{\mathbf{w}}$ become smaller in steady state, and the required k_s to reject the disturbance will be smaller.

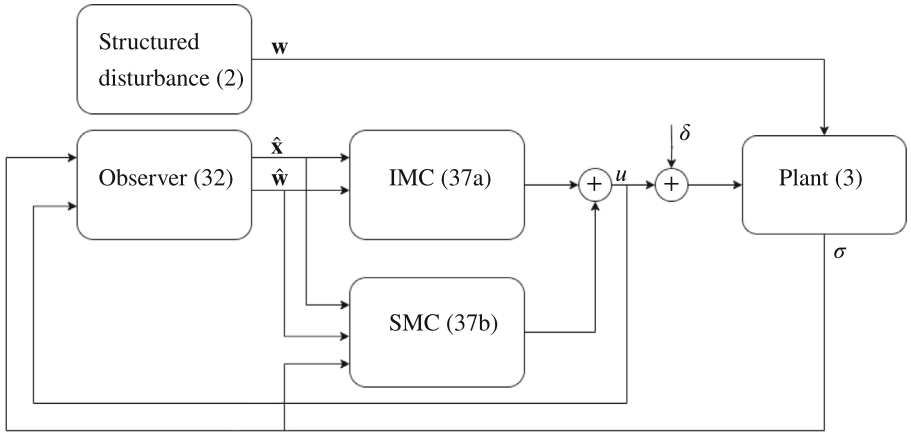

FIGURE 1 Block diagram of the proposed feedback loop structure. It is sketched such that the individual parts contributing to the overall control action u can be identified.

The control input u in (33) is a combination of IMC and SMC parts is given by:

$$u_{\mathrm{I}} = -\mathbf{k}^{\mathrm{T}}\hat{\mathbf{x}} + \mathbf{l}^{\mathrm{T}}\hat{\mathbf{w}}, \tag{37a}$$

$$u_{\mathrm{II}} = -\frac{1}{\mathbf{c}^{\mathrm{T}}\mathbf{b}}\left(\mathbf{c}^{\mathrm{T}}(\mathbf{A}-\mathbf{b}\mathbf{k}^{\mathrm{T}})(\hat{\mathbf{x}}-\boldsymbol{\Pi}\hat{\mathbf{w}}) + k_{\mathrm{s}}\mathrm{sign}(\sigma) + k_{\lambda}\sigma\right). \tag{37b}$$

Figure 1 illustrates the block diagram of the proposed control system (IMSMC) integrating an observer. The IMSMC in (33) is separated into two parts: the internal model-based control (IMC) and the sliding mode control (SMC). Each block is explicitly linked to its corresponding equation to make it more convenient for the reader.

Proof of Theorem 2: At first the boundedness of the estimation error dynamic is investigated. In this regard, the dynamics of the estimation error is represented as

$$\begin{aligned}\dot{\mathbf{e}}_{\mathrm{es}} = \begin{bmatrix}\dot{\mathbf{e}}_{\mathbf{x}}\\ \dot{\mathbf{e}}_{\mathbf{w}}\end{bmatrix} &= \begin{bmatrix}\mathbf{A} & \mathbf{P}\\ \mathbf{0} & \mathbf{S}\end{bmatrix}\begin{bmatrix}\mathbf{x}\\ \mathbf{w}\end{bmatrix} + \begin{bmatrix}\mathbf{b}\\ \mathbf{0}\end{bmatrix}u + \begin{bmatrix}\mathbf{b}\\ \mathbf{0}\end{bmatrix}\delta - \left(\begin{bmatrix}\mathbf{A} & \mathbf{P}\\ \mathbf{0} & \mathbf{S}_{\mathrm{n}}\end{bmatrix} - \begin{bmatrix}\mathbf{g}_1\\ \mathbf{g}_2\end{bmatrix}\left(\begin{bmatrix}\mathbf{c}^{\mathrm{T}} & \mathbf{q}^{\mathrm{T}}\end{bmatrix}\right)\right)\begin{bmatrix}\hat{\mathbf{x}}\\ \hat{\mathbf{w}}\end{bmatrix} - \begin{bmatrix}\mathbf{b}\\ \mathbf{0}\end{bmatrix}u - \begin{bmatrix}\mathbf{g}_1\\ \mathbf{g}_2\end{bmatrix}\sigma =\\ &= \begin{bmatrix}\mathbf{A}-\mathbf{g}_1\mathbf{c}^{\mathrm{T}} & \mathbf{P}-\mathbf{g}_1\mathbf{q}^{\mathrm{T}}\\ -\mathbf{g}_2\mathbf{c}^{\mathrm{T}} & \mathbf{S}_{\mathrm{n}}-\mathbf{g}_2\mathbf{q}^{\mathrm{T}}\end{bmatrix}\begin{bmatrix}\mathbf{e}_{\mathbf{x}}\\ \mathbf{e}_{\mathbf{w}}\end{bmatrix} + \begin{bmatrix}\mathbf{0} & \mathbf{0}\\ \mathbf{0} & \mathbf{S}_{\Delta}\end{bmatrix}\begin{bmatrix}\mathbf{x}\\ \mathbf{w}\end{bmatrix} + \begin{bmatrix}\mathbf{b}\\ \mathbf{0}\end{bmatrix}\delta.\end{aligned} \tag{38}$$

With a proper choice for the observer gains $\mathbf{g}_{\mathrm{i}}$, the dynamic matrix in (38) is Hurwitz and with bounded $\mathbf{S}_{\Delta}$, disturbance $\mathbf{w}$ and δ, the estimation error $\mathbf{e}_{\mathrm{es}}$ is bounded. Now the closed-loop is extracted with combining u from (33) with (3a) and (2). The expanded version of the closed-loop in the observer case is

$$\dot{\mathbf{x}} = \mathbf{A}\mathbf{x} - \mathbf{b}\left(\mathbf{k}^{\mathrm{T}} + \frac{\mathbf{c}^{\mathrm{T}}(\mathbf{A}-\mathbf{b}\mathbf{k}^{\mathrm{T}})}{\mathbf{c}^{\mathrm{T}}\mathbf{b}}\right)\hat{\mathbf{x}} + \mathbf{b}\left(\mathbf{l}^{\mathrm{T}} + \frac{\mathbf{c}^{\mathrm{T}}(\mathbf{A}-\mathbf{b}\mathbf{k}^{\mathrm{T}})\boldsymbol{\Pi}}{\mathbf{c}^{\mathrm{T}}\mathbf{b}}\right)\hat{\mathbf{w}} - \mathbf{b}\frac{k_{\mathrm{s}}\mathrm{sign}(\sigma)}{\mathbf{c}^{\mathrm{T}}\mathbf{b}} + \mathbf{P}\mathbf{w} + \mathbf{b}\delta - \frac{\mathbf{b}k_{\lambda}\mathbf{c}^{\mathrm{T}}}{\mathbf{c}^{\mathrm{T}}\mathbf{b}}\mathbf{x} - \frac{\mathbf{b}k_{\lambda}\mathbf{q}^{\mathrm{T}}}{\mathbf{c}^{\mathrm{T}}\mathbf{b}}\mathbf{w} \tag{39}$$

$$\dot{\mathbf{w}} = \mathbf{S}\mathbf{w}. \tag{40}$$

After replacing $\hat{\mathbf{x}} = \mathbf{x} - \mathbf{e}_{\mathbf{x}}$ in (39), the final version is

$$\begin{aligned}\dot{\mathbf{x}} &= \mathbf{A}\mathbf{x} - \mathbf{b}\mathbf{k}^{\mathrm{T}}\mathbf{x} - \mathbf{b}\frac{\mathbf{c}^{\mathrm{T}}(\mathbf{A}-\mathbf{b}\mathbf{k}^{\mathrm{T}})}{\mathbf{c}^{\mathrm{T}}\mathbf{b}}\mathbf{x} + \mathbf{b}\mathbf{k}^{\mathrm{T}}\mathbf{e}_{\mathbf{x}} + \mathbf{b}\frac{\mathbf{c}^{\mathrm{T}}(\mathbf{A}-\mathbf{b}\mathbf{k}^{\mathrm{T}})}{\mathbf{c}^{\mathrm{T}}\mathbf{b}}\mathbf{e}_{\mathbf{x}} + \mathbf{b}\mathbf{l}^{\mathrm{T}}\mathbf{w} + \mathbf{b}\frac{\mathbf{c}^{\mathrm{T}}(\mathbf{A}-\mathbf{b}\mathbf{k}^{\mathrm{T}})\boldsymbol{\Pi}}{\mathbf{c}^{\mathrm{T}}\mathbf{b}}\mathbf{w}\\ &\quad - \mathbf{b}\mathbf{l}^{\mathrm{T}}\mathbf{e}_{\mathbf{w}} - \mathbf{b}\frac{\mathbf{c}^{\mathrm{T}}(\mathbf{A}-\mathbf{b}\mathbf{k}^{\mathrm{T}})\boldsymbol{\Pi}}{\mathbf{c}^{\mathrm{T}}\mathbf{b}}\mathbf{e}_{\mathbf{w}} - \mathbf{b}\frac{k_{\mathrm{s}}\mathrm{sign}(\sigma)}{\mathbf{c}^{\mathrm{T}}\mathbf{b}} + \mathbf{P}\mathbf{w} + \mathbf{b}\delta - \frac{\mathbf{b}k_{\lambda}\mathbf{c}^{\mathrm{T}}}{\mathbf{c}^{\mathrm{T}}\mathbf{b}}\mathbf{x} - \frac{\mathbf{b}k_{\lambda}\mathbf{q}^{\mathrm{T}}}{\mathbf{c}^{\mathrm{T}}\mathbf{b}}\mathbf{w} =\\ &= \left(\mathbf{A} - \frac{\mathbf{b}\mathbf{c}^{\mathrm{T}}\mathbf{A}}{\mathbf{c}^{\mathrm{T}}\mathbf{b}} - \frac{\mathbf{b}\mathbf{c}^{\mathrm{T}}k_{\lambda}}{\mathbf{c}^{\mathrm{T}}\mathbf{b}}\right)\mathbf{x} + \mathbf{A}_1\mathbf{e}_{\mathbf{x}} + \mathbf{A}_2\mathbf{e}_{\mathbf{w}} + \mathbf{A}_3\mathbf{w} + \mathbf{b}\delta.\end{aligned} \tag{41}$$

In (41), the dynamic matrix is the same as the closed-loop dynamic matrix in (29). Hence this matrix is Hurwitz due to the proof in the previous section. $\mathbf{A}_i$ matrices where $i = 1, 2, 3$ in (41) are constant and have the proper size. Inputs $\mathbf{w}, \mathbf{e_x}, \mathbf{e_w}$ and δ are bounded. As a result, the closed-loop system (41) is stable and consequently the state $\mathbf{x}$ remains bounded.

For the next step, the controller u in (33) is rewritten in terms of the variables $\mathbf{x}, \mathbf{w}, \mathbf{e_x}$ and $\mathbf{e_w}$ instead of $\hat{\mathbf{x}}$ and $\hat{\mathbf{w}}$

$$\begin{aligned} u &= -\mathbf{k}^{\mathrm{T}}\mathbf{x} + \mathbf{l}^{\mathrm{T}}\mathbf{w} + \left(-\frac{\mathbf{c}^{\mathrm{T}}(\mathbf{A}-\mathbf{b}\mathbf{k}^{\mathrm{T}})}{\mathbf{c}^{\mathrm{T}}\mathbf{b}}\right)\mathbf{x} + \left(\frac{\mathbf{c}^{\mathrm{T}}(\mathbf{A}-\mathbf{b}\mathbf{k}^{\mathrm{T}})\mathbf{\Pi}}{\mathbf{c}^{\mathrm{T}}\mathbf{b}}\right)\mathbf{w} + \left(\mathbf{k}^{\mathrm{T}} + \frac{\mathbf{c}^{\mathrm{T}}(\mathbf{A}-\mathbf{b}\mathbf{k}^{\mathrm{T}})}{\mathbf{c}^{\mathrm{T}}\mathbf{b}}\right)\mathbf{e_x} \\ &\quad + \left(-\mathbf{l}^{\mathrm{T}} - \frac{\mathbf{c}^{\mathrm{T}}(\mathbf{A}-\mathbf{b}\mathbf{k}^{\mathrm{T}})\mathbf{\Pi}}{\mathbf{c}^{\mathrm{T}}\mathbf{b}}\right)\mathbf{e_w} - \frac{1}{\mathbf{c}^{\mathrm{T}}\mathbf{b}}(k_{\mathrm{s}}\mathrm{sign}(\sigma) + k_{\lambda}\sigma) = \\ &= -\mathbf{k}^{\mathrm{T}}\mathbf{x} + \mathbf{l}^{\mathrm{T}}\mathbf{w} + u_{\mathrm{s}}. \end{aligned} \tag{42}$$

In (42), all the elements except $\mathbf{k}^{\mathrm{T}}\mathbf{x}$ and $\mathbf{l}^{\mathrm{T}}\mathbf{w}$ are summarized in u_{s}. Then the first time derivative of the output σ is computed with u from (42), that is,

$$\begin{aligned} \dot{\sigma} &= \mathbf{c}^{\mathrm{T}}\big((\mathbf{A}-\mathbf{b}\mathbf{k}^{\mathrm{T}})\mathbf{x} + (\mathbf{b}\mathbf{l}^{\mathrm{T}} + \mathbf{P})\mathbf{w} + \mathbf{b}u_{\mathrm{s}}\big) + \mathbf{c}^{\mathrm{T}}\mathbf{b}\delta + \mathbf{q}^{\mathrm{T}}\mathbf{S}\mathbf{w} = \\ &= \mathbf{c}^{\mathrm{T}}\big((\mathbf{A}-\mathbf{b}\mathbf{k}^{\mathrm{T}})(\tilde{\mathbf{x}} + \mathbf{\Pi}\mathbf{w}) + (\mathbf{b}\mathbf{l}^{\mathrm{T}} + \mathbf{P})\mathbf{w}\big) + \mathbf{c}^{\mathrm{T}}\mathbf{b}\delta + \mathbf{q}^{\mathrm{T}}\mathbf{S}\mathbf{w} + \mathbf{c}^{\mathrm{T}}\mathbf{b}u_{\mathrm{s}} = \\ &= \mathbf{c}^{\mathrm{T}}(\mathbf{A}-\mathbf{b}\mathbf{k}^{\mathrm{T}})\tilde{\mathbf{x}} + \mathbf{c}^{\mathrm{T}}\mathbf{b}\delta + \mathbf{q}^{\mathrm{T}}\mathbf{S}_{\Delta}\mathbf{w} + \mathbf{c}^{\mathrm{T}}\mathbf{b}u_{\mathrm{s}} = \\ &= \mathbf{q}^{\mathrm{T}}\mathbf{S}_{\Delta}\mathbf{w} + \big(\mathbf{c}^{\mathrm{T}}\mathbf{b}\mathbf{k}^{\mathrm{T}} + \mathbf{c}^{\mathrm{T}}(\mathbf{A}-\mathbf{b}\mathbf{k}^{\mathrm{T}})\big)\mathbf{e_x} - \big(\mathbf{c}^{\mathrm{T}}\mathbf{b}\mathbf{l}^{\mathrm{T}} + \mathbf{c}^{\mathrm{T}}(\mathbf{A}-\mathbf{b}\mathbf{k}^{\mathrm{T}})\mathbf{\Pi}\big)\mathbf{e_w} + \mathbf{c}^{\mathrm{T}}\mathbf{b}\delta - (k_{\mathrm{s}}\mathrm{sign}(\sigma) + k_{\lambda}\sigma) = \\ &= \Delta_{\mathrm{obsv}} - (k_{\mathrm{s}}\mathrm{sign}(\sigma) + k_{\lambda}\sigma). \end{aligned} \tag{43}$$

The function Δ_{obsv} from (43) consists of a part similar to Δ in (27) which is bounded and the upper bound is known. Other parts in Δ_{obsv} have known matrices as coefficient to estimation errors $\mathbf{e_x}$ and $\mathbf{e_w}$ which also are bounded. From (38), the maximum absolute value for the estimation error can be extracted and with all the information, Δ_{Max} is known. As a result, and similar to the previous section, the sliding mode part within the control signal is capable to compensate Δ_{obsv} and reject the disturbance in observer case in finite time.[24] □

4 | SIMULATION STUDY

In this section, the proposed method is applied on an integrated active-suspension-system for a quarter-car model in order to observe the practicality of the proposed control concept. Figure 2 shows the schematic of the considered action-suspension system.

The upper mass M_{s} in Figure 2 represents the car body (suspended mass) and M_{us} represents the car tire (un-suspended mass). The connection between these two masses and the tire and the bumpy ground are simulated via a spring damper system with damper coefficients B_{s} and B_{us}, and spring coefficients K_{s} and K_{us}. The DC-motor between M_{s} and M_{us} is the control input for the plant. In general, the goal is to control the DC-motor such that the impact of the disturbance induced by an uneven ground onto the car and its driver is compensated. In other words, the movement of the upper mass M_{s} should be as small as possible. After deriving the equations of motion for both masses and defining new states, the final state-space representation is

$$\begin{aligned} \dot{\mathbf{x}} &= \begin{bmatrix} 0 & 1 & 0 & -1 \\ -\frac{K_{\mathrm{s}}}{M_{\mathrm{s}}} & -\frac{B_{\mathrm{s}}}{M_{\mathrm{s}}} & 0 & \frac{B_{\mathrm{s}}}{M_{\mathrm{s}}} \\ 0 & 0 & 0 & 1 \\ \frac{K_{\mathrm{s}}}{M_{\mathrm{us}}} & \frac{B_{\mathrm{s}}}{M_{\mathrm{us}}} & -\frac{K_{\mathrm{us}}}{M_{\mathrm{us}}} & -\frac{B_{\mathrm{s}}+B_{\mathrm{us}}}{M_{\mathrm{us}}} \end{bmatrix}\mathbf{x} + \begin{bmatrix} 0 \\ \frac{1}{M_{\mathrm{s}}} \\ 0 \\ -\frac{1}{M_{\mathrm{us}}} \end{bmatrix} u + \begin{bmatrix} 0 \\ 0 \\ -1 \\ \frac{B_{\mathrm{us}}}{M_{\mathrm{us}}} \end{bmatrix}\eta, \\ \sigma &= \begin{bmatrix} 0 & 1 & 0 & 0 \end{bmatrix}\mathbf{x}, \end{aligned} \tag{44}$$

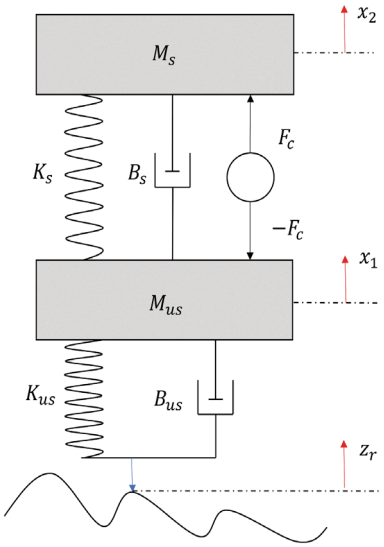

FIGURE 2 Active-suspension-system used for simulation studies. In the given system, the upper mass represents the mass of the vehicle body, while the lower mass represents the mass of the tire. The connection between the two masses is modeled using a simple spring-damper system. The control input applies an equal force in opposite directions to both masses. Additionally, the connection between the tires and the bumpy road is also modeled using a spring-damper system.

where

$$\mathbf{x} = \begin{bmatrix} x_2 - x_{2,\mathrm{RL}} - \left(x_1 - x_{1,\mathrm{RL}}\right) \\ \dot{x}_2 - \dot{x}_{2,\mathrm{RL}} \\ x_1 - x_{1,\mathrm{RL}} - z_{\mathrm{r}} \\ \dot{x}_1 - \dot{x}_{1,\mathrm{RL}} \end{bmatrix} \tag{45}$$

is defined with the help of equilibrium points

$$\begin{aligned} x_{1,\mathrm{RL}} &= -\frac{(M_{\mathrm{s}} + M_{\mathrm{us}})g}{K_{\mathrm{us}}}, \\ x_{2,\mathrm{RL}} &= -\frac{M_{\mathrm{s}}g}{K_{\mathrm{s}}} - \frac{(M_{\mathrm{s}} + M_{\mathrm{us}})g}{K_{\mathrm{us}}}, \end{aligned} \tag{46}$$

in order to eliminate the gravitational force in state space representation. In (44), the sliding variable σ is the tracking error. In (45), x_1 represents the movement of the car tire, x_2 indicates the displacement of the car body, and z_r describes the movement of the entire system relative to the bumpy road. The values for the parameters in (44) are given in Table 1. In (44)

$$\eta = 0.003 \sin(\omega t) \tag{47}$$

is the disturbance and ω comes from the exosystem. To make the simulation more interesting, a reference $-\mathbf{q}^{\mathrm{T}}\mathbf{w}$ is introduced. At the end, the system in (44) is represented similar to (3) as

$$\dot{\mathbf{x}} = \mathbf{A}\mathbf{x} + \mathbf{b}u + \mathbf{P}\mathbf{w}, \tag{48a}$$

$$\sigma = \mathbf{c}^{\mathrm{T}}\mathbf{x} + \mathbf{q}^{\mathrm{T}}\mathbf{w}, \tag{48b}$$

TABLE 1 Active-suspension-system parameters which are used in the same setup as in Reference [27].

Symbol	Nominal value	Unit
K_s	1040	Nm^{-1}
K_{us}	2300	Nm^{-1}
M_s	2	kg
M_{us}	1.15	kg
B_s	2	Nsm^{-1}
B_{us}	1	Nsm^{-1}

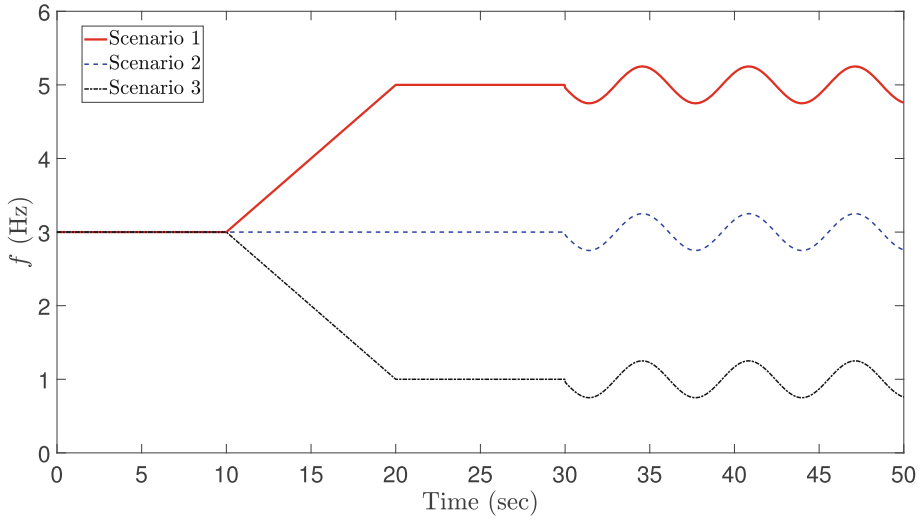

FIGURE 3 Profile of the employed disturbance frequency. In the first cenario, the disturbance frequency starts at 3 Hz and gradually increases over a period of 10 s, reaching 5 Hz by the 20-s mark. Scenario 3 is similar to this one except it reaches to 1 Hz instead of 5 Hz and for Scenario 2, the frequency remains constant at 3 Hz. A periodic change, starting at $t = 30$ s, is also added to each scenario (MATLAB/Simulink, ode3, step size : $T_s = 10^{-4}$s).

where

$$\mathbf{A} = \begin{bmatrix} 0 & 1 & 0 & -1 \\ -\frac{K_s}{M_s} & -\frac{B_s}{M_s} & 0 & \frac{B_s}{M_s} \\ 0 & 0 & 0 & 1 \\ \frac{K_s}{M_{us}} & \frac{B_s}{M_{us}} & -\frac{K_{us}}{M_{us}} & -\frac{B_s+B_{us}}{M_{us}} \end{bmatrix}, \quad \mathbf{b} = \begin{bmatrix} 0 \\ \frac{1}{M_s} \\ 0 \\ -\frac{1}{M_{us}} \end{bmatrix}, \quad \mathbf{P} = \begin{bmatrix} 0 & 0 \\ 0 & 0 \\ -0.003 & 0 \\ 0.003\frac{B_{us}}{M_{us}} & 0 \end{bmatrix},$$
$$\mathbf{c}^T = \begin{bmatrix} 0 & 1 & 0 & 0 \end{bmatrix}, \quad \mathbf{q}^T = \begin{bmatrix} 0.1 & 0 \end{bmatrix}. \tag{49}$$

Three scenarios are defined to compare the performance of the IMC, SMC and IMSMC. In the first one, the frequency of the disturbance is set to 3 Hz and after 10 s, it reaches to 5 Hz. In the second scenario, the frequency stays at 3 Hz and in the last one it starts from 3 Hz and ends at 1 Hz. At the end of each scenario, a periodic alteration is included. Figure 3 shows the profile of the frequency time evolution for each case.

The nominal frequency for IMSMC method is 3 Hz. The matrices $\mathbf{S}_n$ and $\mathbf{S}_\Delta(t)$ are

$$\mathbf{S}_n = 2\pi \begin{bmatrix} 0 & 3 \\ -3 & 0 \end{bmatrix}, \tag{50}$$

$$\mathbf{S}_{\Delta}(t) = 2\pi \begin{cases} \begin{bmatrix} 0 & 0 \\ 0 & 0 \end{bmatrix}, & t \le 10, \\ \begin{bmatrix} 0 & f_m(t-10) \\ -f_m(t-10) & 0 \end{bmatrix}, & 10 < t \le 20, \\ \begin{bmatrix} 0 & 10f_m \\ -10f_m & 0 \end{bmatrix}, & 20 < t \le 30, \\ \begin{bmatrix} 0 & f_n + 0.25sin\left(t + \frac{3\pi}{2}\right) \\ -\left(f_n + 0.25sin\left(t + \frac{3\pi}{2}\right)\right) & 0 \end{bmatrix}, & 30 < t, \end{cases} \tag{51}$$

where for Scenario 1, $f_m = 0.2$ and $f_n = 5$, for Scenario 2, $f_m = 0$ and $f_n = 3$, and for Scenario 3, $f_m = -0.2$ and $f_n = 1$. The unit for time t in (51) is second. The initial state $\mathbf{x}(0) = \begin{bmatrix} 0 & 0 & 0 & 0 \end{bmatrix}^{\mathrm{T}}$ and initial disturbance is $\mathbf{w}(0) = \begin{bmatrix} 0 & 1 \end{bmatrix}^{\mathrm{T}}$. The simulation is run in Matlab/Simulink environment with a fixed step size of 10^{-4} second using the ode3 solver. The IMC controller is designed to place the eigenvalues of the unperturbed system at $\begin{bmatrix} -20 & -20 & -20 & -20 \end{bmatrix}$ and the Luenberger observer gain is tuned to place the eigenvalues of the dynamic matrix in (32) at $\begin{bmatrix} -50 & -50 & -50 & -50 & -50 & -50 \end{bmatrix}$. The vector $\mathbf{l}$ and the matrix $\mathbf{\Pi}$ is computed by solving the regulator Equations (7). For the SMC, the controller is in the form

$$u_{\mathrm{SMC}} = -\mathbf{k}^{\mathrm{T}}\hat{\mathbf{x}} + -\frac{1}{\mathbf{c}^{\mathrm{T}}\mathbf{b}}\left[\mathbf{c}^{\mathrm{T}}(\mathbf{A} - \mathbf{b}\mathbf{k}^{\mathrm{T}})\hat{\mathbf{x}} + k_{s_{\mathrm{SMC}}}\mathrm{sign}(\sigma)\right], \tag{52}$$

where $\mathbf{k}$ is the same in all three controllers. For the sliding mode controller

$$\Delta_{\mathrm{obsv}} = \mathbf{c}^{\mathrm{T}}\mathbf{P}\mathbf{w} + \mathbf{q}^{\mathrm{T}}\mathbf{S}\mathbf{w} + \mathbf{c}^{\mathrm{T}}\mathbf{A}\mathbf{e}_{\mathbf{x}}. \tag{53}$$

Figure 4 depicts Δ_{obsv} of the IMSMC and SMC for each scenario. Except the initial phase of the simulation, Δ_{obsv} is significantly smaller for the IMSMC compared to the SMC method. This will lead to smaller k_s in the controller and eventually smaller control input effort.

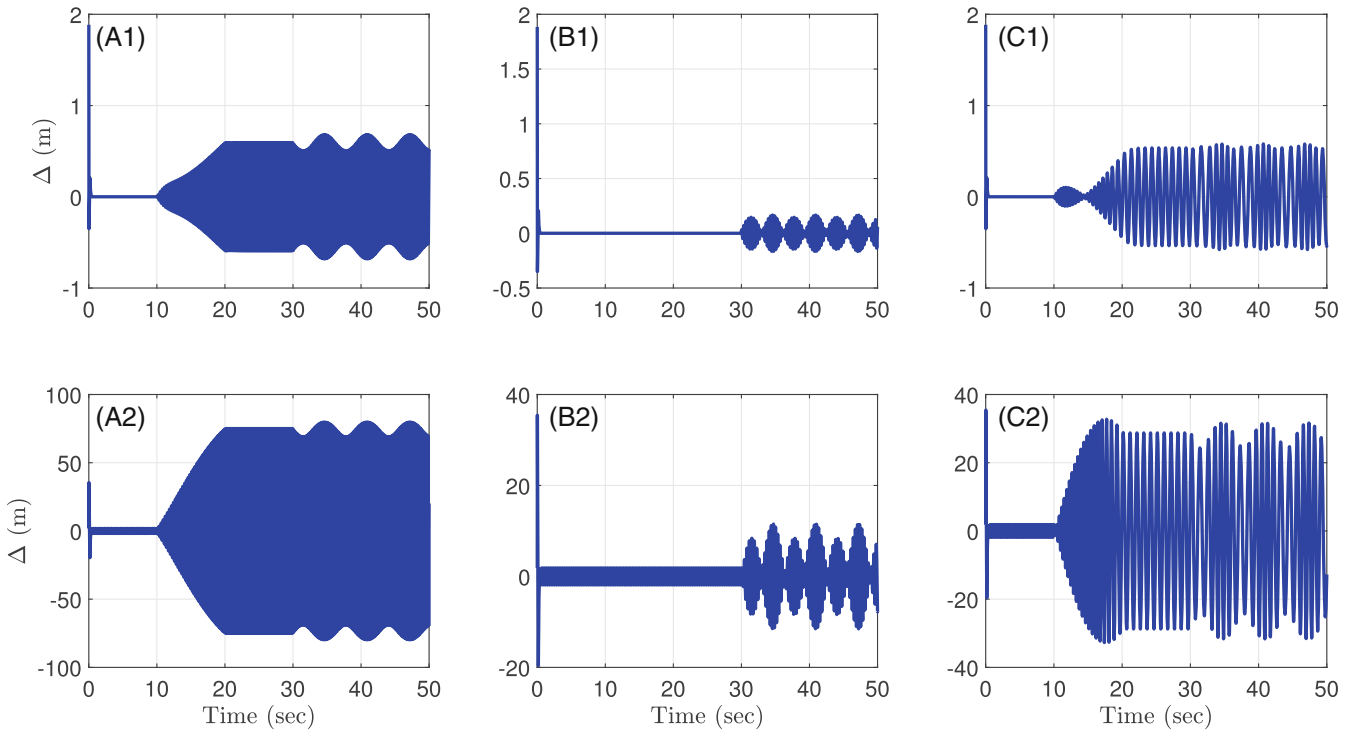

FIGURE 4 The profile of Δ derived from Equations (35) and (53), across various scenarios. Subfigures (A1), (B1), and (C1) represent Δ values for the IMSMC method from equation (35) in Scenarios 1, 2, and 3, respectively. Similarly, (A2), (B2), and (C2) depict Δ values for the SMC method from Equation (53) in the same scenarios. Notably, the Δ values for the IMSMC method are consistently lower than those for the SMC method across all scenarios. This difference enables the selection of smaller k_s and a reduced control effort when using the IMSMC method compare to the SMC method (MATLAB/Simulink, ode3, step size : $T_s = 10^{-4}$ s).

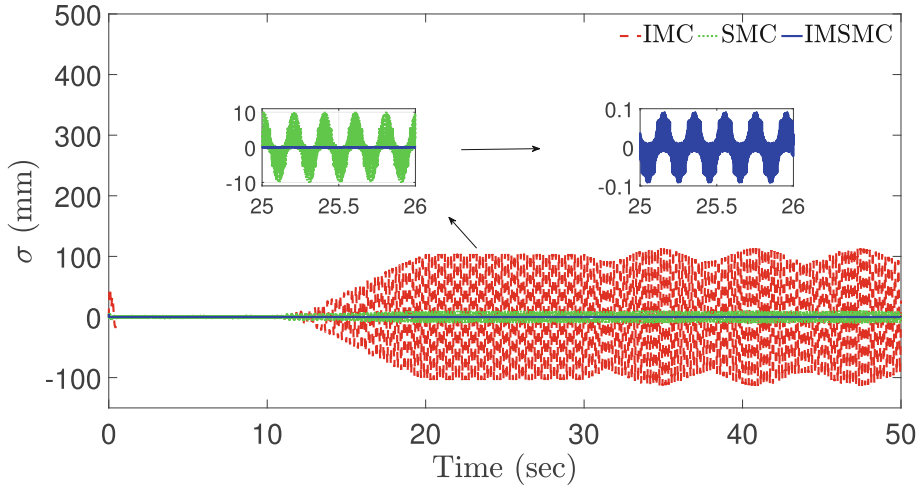

FIGURE 5 The tracking error σ for three control methods in Scenario 1. Initially, during the first 10 s when there is no uncertainty in the exosystem, all three controllers perform adequately. However, after 10 s, when uncertainty is introduced to the exosystem, the IMC method fails to reject the disturbance, leading to an increased tracking error. In contrast, both the IMSMC and SMC methods keep the tracking error within a narrow range. The zoomed-in plots reveal that the tracking error boundary for the SMC method is significantly larger than that for the IMSMC, demonstrating the IMSMC's superior ability to minimize tracking error (MATLAB/Simulink, ode3, step size : $T_s = 10^{-4}$s).

Figure 5 till 10 provide a comprehensive comparison of the three control methods—IMC, IMSMC, and SMC—across varying scenarios, specifically highlighting tracking errors and control efforts under different conditions of uncertainty within the exosystem. Figures 5–7 focus on the tracking error σ. In Figure 5, during the initial 10 s without uncertainty, all controllers perform adequately. However, once uncertainty is introduced, the IMC's performance in rejecting disturbances deteriorates, leading to an increased tracking error. In contrast, the IMSMC and SMC manage to maintain the tracking error within a much narrower range. The zoomed-in plots in this figure allow for a detailed observation, showing that the tracking error boundary for the IMSMC is significantly tighter than that of the SMC, demonstrating its enhanced capability to maintain precision in the uncertain case. Figure 6 continues this theme in a different scenario. For the initial 30 s, all methods cope well, but the subsequent introduction of uncertainty again deteriorates the IMC's performance. The zoomed-in plots in this figure clearly highlight that the IMSMC maintains a narrower tracking error band than the SMC, showcasing its consistent reliability and superior disturbance rejection properties. In Figure 7, the pattern repeats with all controllers rejecting the disturbance in the absence of uncertainty. The introduction of uncertainty impacts the IMC performance, causing a notable increase in tracking error, while the IMSMC and SMC remain robust. The zoomed-in portion of Figure 7 emphasizes the lower boundary of the tracking error for the IMSMC as compared to the SMC, reiterating the IMSMC's superior handling and efficiency in response control.

The control efforts illustrated in Figures 8–10 depict the extent of effort each method utilizes in each scenario. Figure 8 shows that the SMC's larger control actions, dictated by the larger values of Δ, require a higher k_s value. The zoomed-in plot highlights that while the IMSMC's control input is comparable to the IMC, it achieves significantly better outcomes in terms of a reduced tracking error, as seen in Figure 5. This plot provides a clear visual contrast in the efficiency of control efforts between the methods. In Figure 9, similar to the first scenario, the SMC requires a larger control effort to manage disturbances compared to the IMSMC and IMC, with the IMSMC's control input lying between the IMC's and SMC's. The detailed zoomed-in view illustrates how the selection of k_s value and the corresponding profile of Δ influence the control boundaries, showing a smaller effort by the IMSMC compared to the SMC. Finally, Figure 10 captures the scenario where the SMC again shows a higher control input requirement. The zoomed-in plot provides a graphical representation that despite the IMSMC and IMC having comparable control efforts, the IMSMC's performance in minimizing tracking error remains superior, especially as depicted in Figure 7. These figures collectively reveal that while the IMC struggles with increasing uncertainty, the IMSMC exhibits a consistent ability to balance control effort with effective disturbance rejection showing clear superiority over the IMC and the SMC.

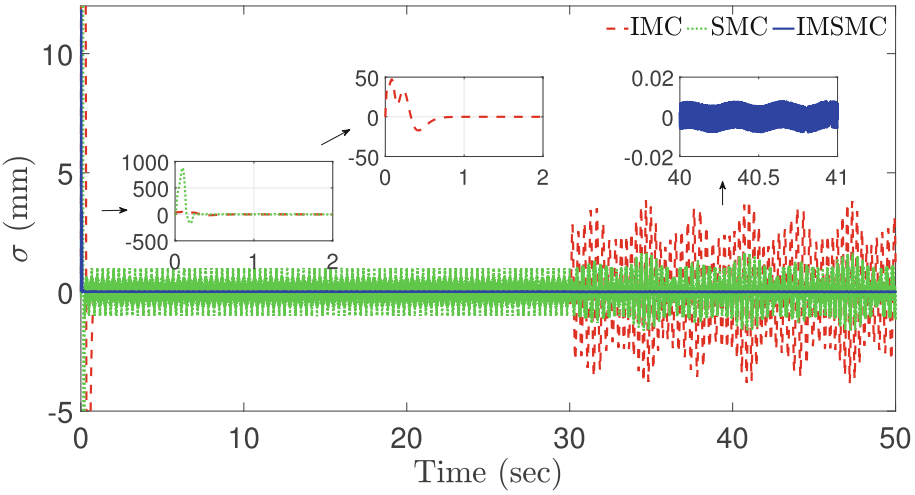

FIGURE 6 The tracking error σ for three control methods in Scenario 2. For the first 30 s, without uncertainty in the exosystem, all methods perform adequately. The initial behavior of the IMC remains consistent across all scenarios, whereas the performance of the other two methods varies with changes in k_s for each scenario. The introduction of uncertainty at 30 s adversely affects the IMC's performance. The zoomed-in plot highlights that the IMSMC maintains a narrower tracking error band compared to the SMC method (MATLAB/Simulink, ode3, step size : $T_s = 10^{-4}$ s).

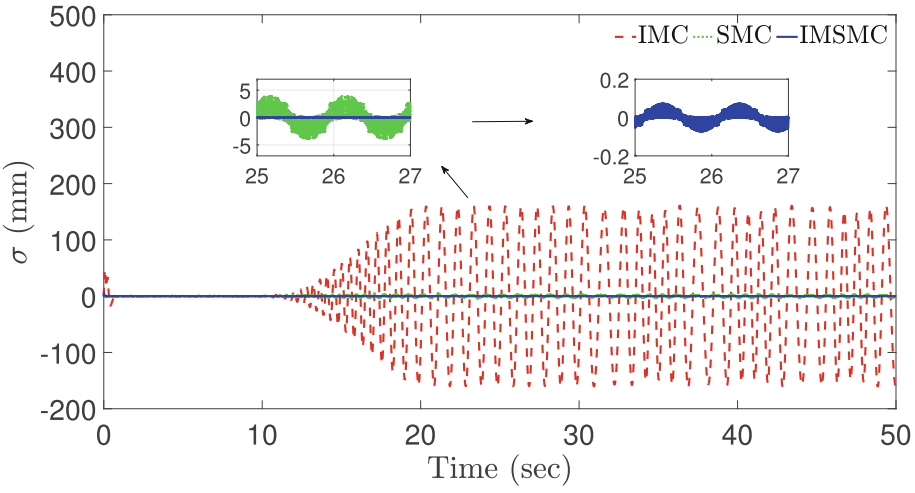

FIGURE 7 The tracking error σ for three control methods in Scenario 3. Initially, up to 10 s with no uncertainty in the exosystem, all three controllers effectively reject the disturbance. However, upon the introduction of uncertainty, the IMC struggles to minimize the disturbance's impact, whereas the IMSMC and SMC maintain their effectiveness. The zoomed-in plot reveals a lower tracking error boundary for the IMSMC compared to the SMC, highlighting the IMSMC's advantage over the other methods (MATLAB/Simulink, ode3, step size : $T_s = 10^{-4}$ s).

For further investigation, the proposed method performance is compared to a robust IMC controller: Adaptive IMC. The gains of adaptive IMC is tuned for the first scenario in Figure 3, and for preventing divergence in the tracking error σ across all scenarios, $\mathbf{q}^T = \begin{bmatrix}0 & 0\end{bmatrix}$ is considered. The tuning parameters of the adaptive algorithm in Reference 11 are set to $K_f = 0.4788$, $K_e = 0.1$ and $y_a = \begin{bmatrix}0 & 1 & 0\end{bmatrix}$. The initial value for ζ is set to $\begin{bmatrix}0 & 0.00001 & 0\end{bmatrix}^T$. Figure 11 till 13 depict the tracking error σ for both methodologies in each scenario in Figure 3. The newly proposed method exhibits a notably small steady-state error for σ, indicating successful disturbance rejection by the controller. In Scenario 1, where the system is subjected to an uncertain disturbance, the adaptive IMC method exhibits a longer response time compared to the IMSMC. The steady-state output for the adaptive IMC is higher, particularly around the 7th to 8th second, indicating less effective

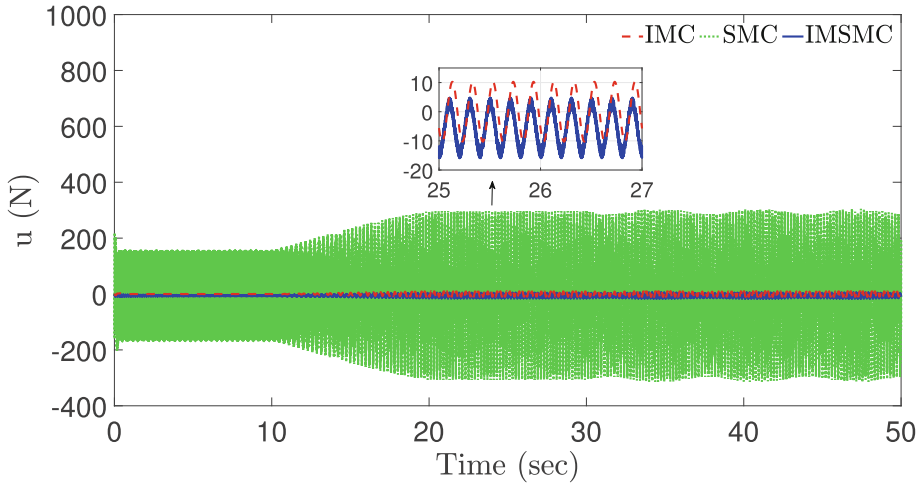

FIGURE 8 The control effort u for three control methods in Scenario 1. The SMC method's control action is significantly larger than the other two methods, due to the large values of Δ as shown in Figure 4, necessitating larger k_s value. The zoomed-in plot indicates that the control input for the IMSMC is comparable to that of the IMC. Despite this, the IMSMC achieves better performance in minimizing tracking error, as detailed in Figure 5. The smaller range of Δ for the IMSMC in Figure 4 supports the lower control effort compared to the SMC (MATLAB/Simulink, ode3, step size : $T_s = 10^{-4}$ s).

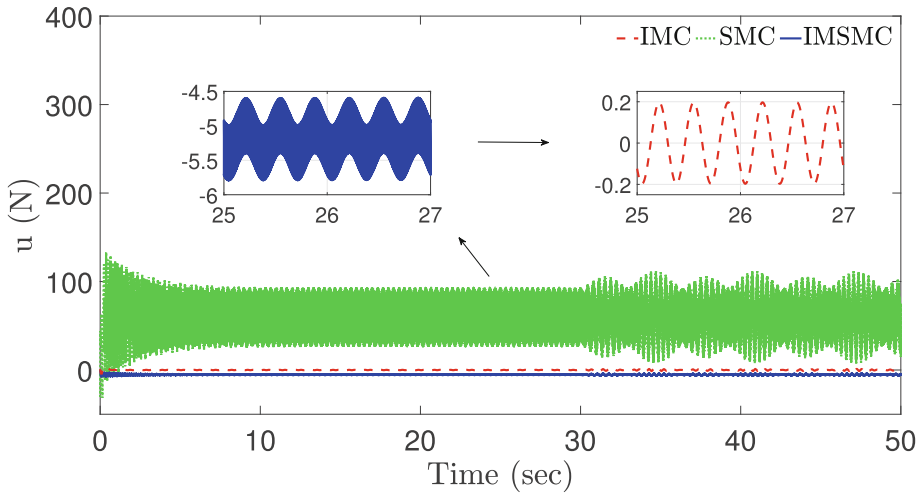

FIGURE 9 The control effort u for three control methods in Scenario 2. As in the first scenario, the SMC method necessitates a larger control effort to reject the disturbance compared to the other two methods. In this scenario, the IMSMC control input is greater than that of the IMC but considerably smaller than that of the SMC. The control effort boundaries for the IMSMC and SMC are directly influenced by the selection of k_s values and the corresponding profile of Δ shown in Figure 4 (MATLAB/Simulink, ode3, step size : $T_s = 10^{-4}$ s).

disturbance handling. The IMSMC, on the other hand, maintains a lower steady-state output, demonstrating superior performance in managing periodic disturbances. In Scenario 2, both the methods show effective disturbance rejection. However, the response time for the adaptive IMC is still larger than the IMSMC which is depicted in the first 5 s of the Figure 12. After 20 s the adaptive IMC performance is deteriorated although the frequency of the disturbance is constant during this phase. Hence, in this scenario, which is the nominal case, the frequency estimate does not converge. After 30 s the output for adaptive IMC deviates due to time-varying frequency in the disturbance. This behavior is also apparent in the Scenario 3 in Figure 13.

The control input u for both methods across the three scenarios further illustrates the differences in their control strategies. In Scenario 1 in Figure 14 the proposed IMSMC method shows a higher frequency of control input signals

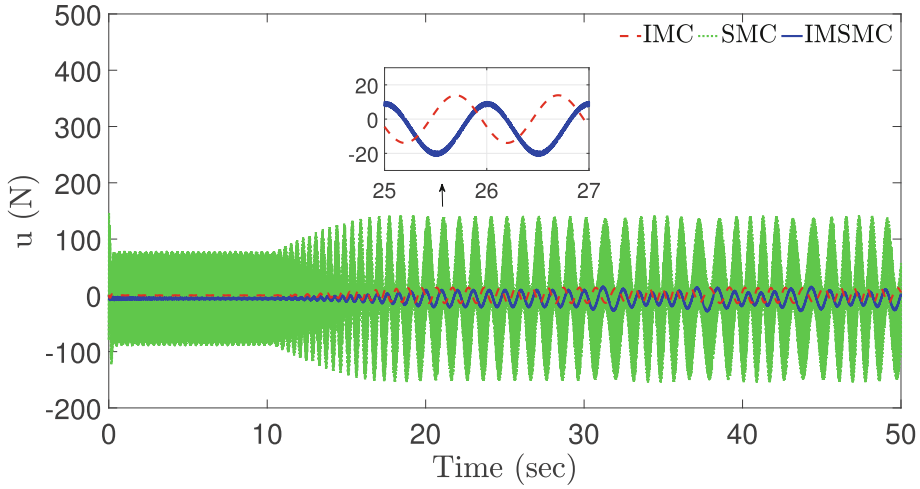

FIGURE 10 The control effort u for three control methods in Scenario 3. The SMC method exhibits a larger control input than the other two methods, due to the selection of larger k_s value. The zoomed-in plot reveals that the control effort bounds for both the IMC and the IMSMC are within the same range. Notably, the IMSMC demonstrates superior performance in minimizing tracking error, as shown in Figure 7, with a control effort comparable to the IMC and significantly smaller than that of the SMC (MATLAB/Simulink, ode3, step size : $T_s = 10^{-4}$ s).

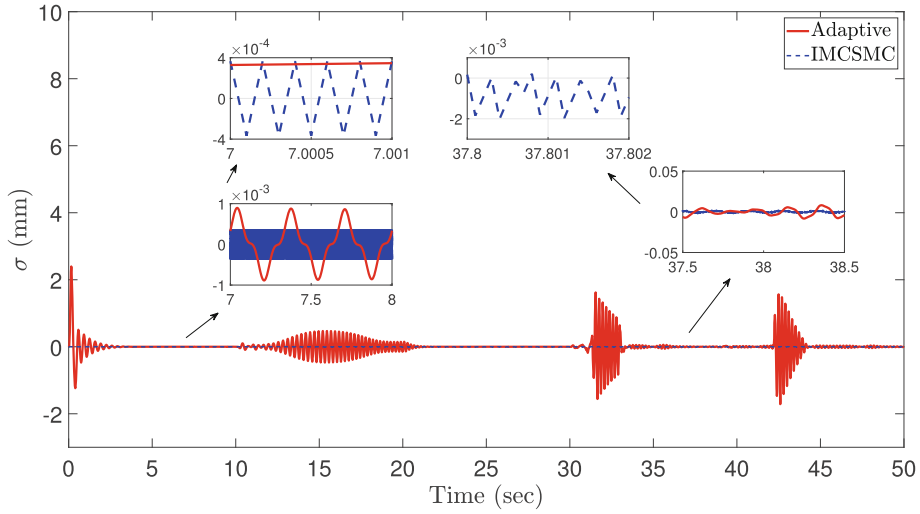

FIGURE 11 Tracking error for both methods in Scenario 1. When employing adaptive IMC, the system takes a longer time to respond to the uncertain disturbance compared to IMSMC. Additionally, the steady-state output is smaller in the proposed approach compared to adaptive IMC, for example, around the 7 to 8 s mark of the simulation. For the periodic disturbance, the IMSMC demonstrates significant performance compare to adaptive IMC (MATLAB/Simulink, ode3, step size : $T_s = 10^{-4}$ s).

compared to the adaptive IMC, a characteristic trait of sliding mode control. The upper bound of the control input for adaptive IMC is slightly larger, whereas the lower bound for IMSMC is much smaller, indicating a broader range of control effort required in IMSMC. In Scenario 2 in Figure 15 the control input behavior remains consistent with Scenario 1. The adaptive IMC method shows a slight deviation from the desired control input after 20 s, indicating the controller's attempt to correct the output trajectory. The IMSMC continues to demonstrate higher frequency control inputs, reflecting its robust and rapid response characteristics. In Scenario 3 in Figure 16 where the actual disturbance frequency is lower than the nominal frequency used in the IMC method, a significant increase in control effort is required to reject the disturbance and maintain the output at zero. This increased effort is observed from 15 s until the end of the simulation. The adaptive IMC method shows a noticeable increase in control input between 25 and 30 s as it attempts to mitigate the large output deviations, whereas the IMSMC manages this more effectively with a consistent control effort.

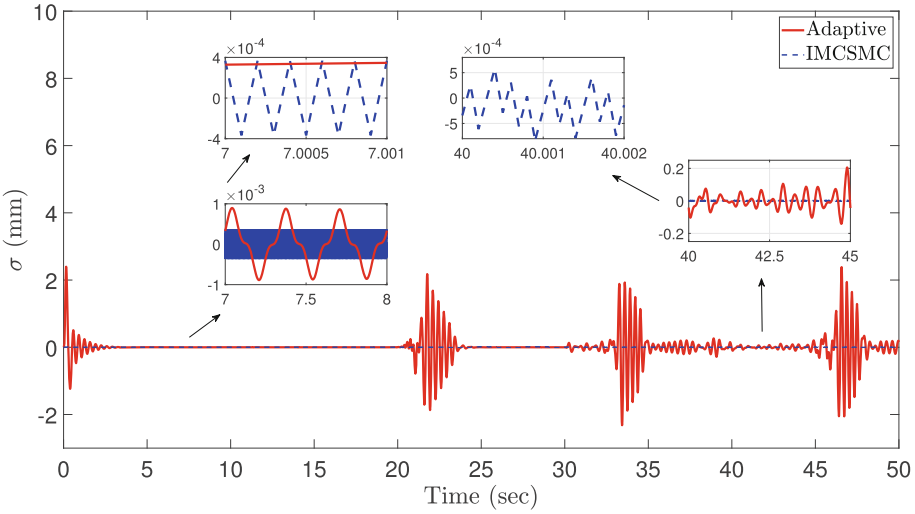

FIGURE 12 Tracking error for both methods in Scenario 2. In Scenario 2 without disturbance uncertainty, both the IMSMC and the adaptive IMC method demonstrate effective disturbance rejection similar to the standard IMC approach. However, the adaptive IMC method exhibits performance similar to Scenario 1 with longer response time and after 20 s, the output deviates from zero for a short time. Besides, the performance of adaptive one is not comparable to IMSMC at the end of simulation (MATLAB/Simulink, ode3, step size : $T_s = 10^{-4}$s).

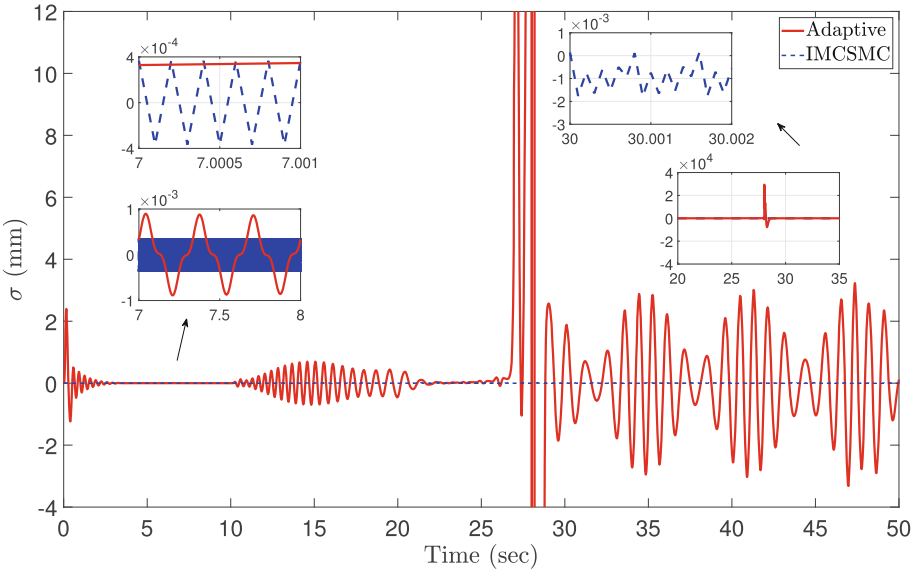

FIGURE 13 Tracking error for both methods in Scenario 3. Both methods, exhibit a response similar to that observed in Scenario 1. However, in the case of the adaptive IMC method, a longer deviation from the desired response is observed, specifically within the 10 to 20 s time interval of the simulation, compared to the response in Scenario 1. Also the output in adaptive IMC from 25 to 30 s of the simulation time become significantly large. It indicates the poor performance of the adaptive method in tackling the disturbance (MATLAB/Simulink, ode3, step size : $T_s = 10^{-4}$s).

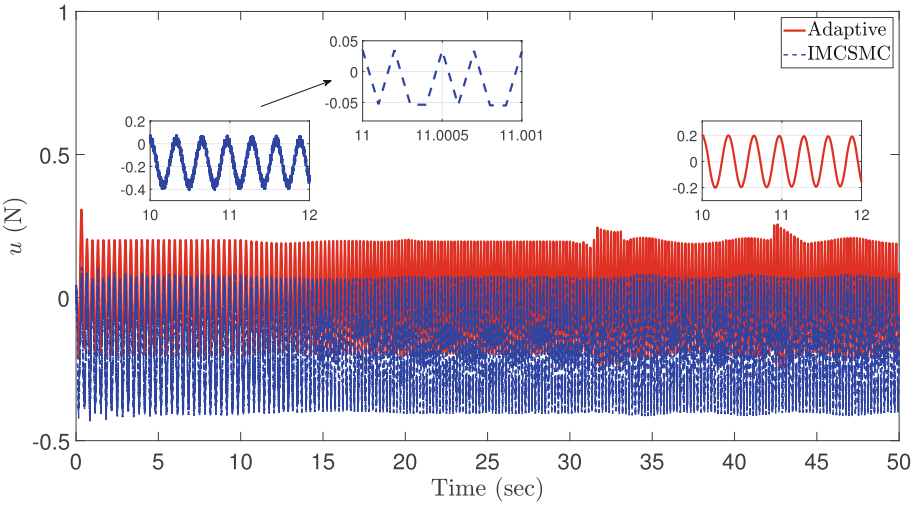

FIGURE 14 Control Input for both methods in Scenario 1. In the proposed method, there is a trade-off when using sliding mode control (IMSMC) compared to adaptive IMC. The frequency of the input signal for IMSMC is significantly higher than that for adaptive IMC. This difference in frequency is a characteristic of using sliding mode control. Additionally, the upper bound of the input signal in the adaptive IMC case is slightly larger than that of IMSMC. Conversely, the lower bound for IMSMC is much smaller compared to the lower bound of the other method (MATLAB/Simulink, ode3, step size : $T_s = 10^{-4}$s).

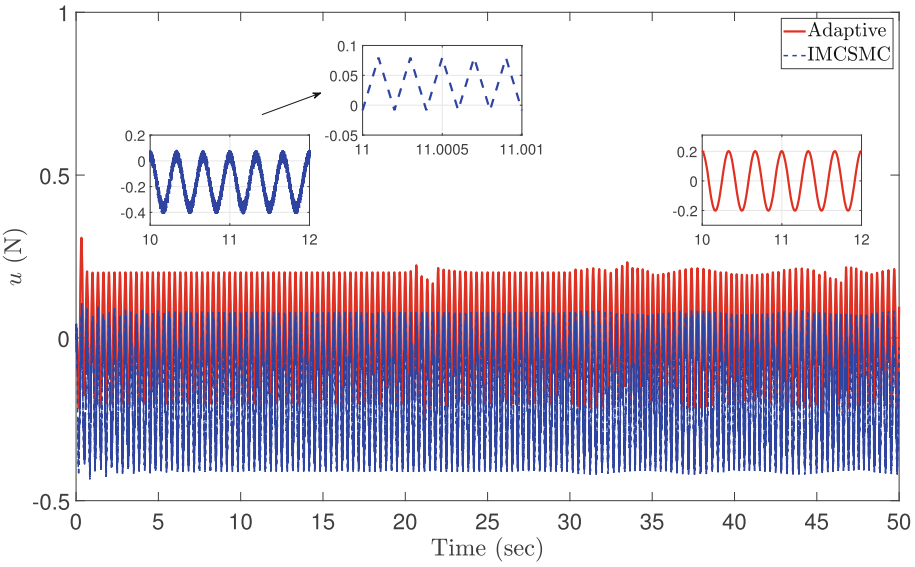

FIGURE 15 Control Input for both methods in Scenario 2. Similar behavior is observed between Scenario 2 and 1. In the adaptive IMC method, a slight deviation from the desired response is noticeable after 20 s. This can be interpreted as the controller's attempt to reduce the deviation in the output and bring it back to the desired trajectory (MATLAB/Simulink, ode3, step size : $T_s = 10^{-4}$s).

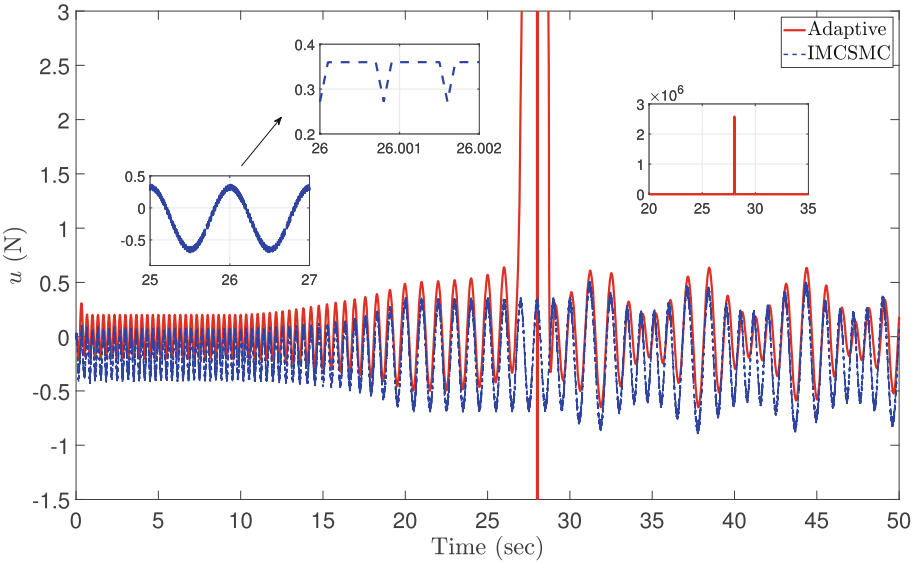

FIGURE 16 Control Input for both methods in Scenario 3. The actual frequency of the disturbance is smaller than the nominal one used in the IMC method. It requires more control effort to reject the disturbance and maintain the output at zero. This increased control effort can be observed from 15 s until the end of the simulation, as the controller compensates for the mismatch between the actual and nominal frequencies to achieve the desired output response. For adaptive IMC between 25 and 30 s, the increase of control input is apparent where the controller attempts to diminish the large output value of the system (MATLAB/Simulink, ode3, step size : $T_s = 10^{-4}$s).

5 | CONCLUSIONS AND FUTURE WORK

This article tackles the challenge of uncertainties in the exosystem used to model external disturbances within the internal model-based control design methodology. To overcome the limitations mentioned in the introduction, this article proposes a novel approach that combines sliding mode control with internal model-based control. By leveraging the advantages of fast disturbance rejection and simplicity in design offered by sliding mode control, the proposed approach provide a robust controller for uncertainty in the disturbance model. Through simulation, the results demonstrate significant improvements compared to the IMC, SMC and adaptive IMC methods. The proposed approach exhibits enhanced performance in terms of disturbance rejection and robustness, showcasing its potential in addressing the inherent uncertainties associated with disturbances. Overall, this research presents a novel approach that effectively addresses the challenge of uncertainties in the model of the disturbance within the internal model-based control strategy. The findings highlight the advantages of combining sliding mode control with internal model-based control and underscore the potential for developing more robust and efficient control solutions in the presence of disturbance uncertainties. While this study has provided meaningful insights into the control of systems with uncertain exosystems and unmatched disturbances, several areas remain open for future research. These include:

- *Discrete-Time Domain Investigation*: Most application-based controllers are implemented in the discrete-time domain. Expanding the proposed controller into this domain is important to enhance its applicability.
- *Higher-order sliding mode controller*: In order to relax the relative degree assumption in the proposed controller and take into account the chattering effect of the sliding mode controllers, the investigation of higher-order sliding mode combined with the IMC is crucial.
- *Experimental Validation*: Conducting experimental validation on systems will be crucial to demonstrate the practical applicability and robustness of the proposed method.
- *Nonlinear Systems*: Since most systems are inherently nonlinear and may not be linearized, analyzing nonlinear systems facing unknown periodic disturbances is another important future direction.

ACKNOWLEDGMENTS

The authors would like to thank Dr. Richard Seeber for the valuable discussions and his constructive feedback.

CONFLICT OF INTEREST STATEMENT

The authors declare no conflicts of interest.

DATA AVAILABILITY STATEMENT

The data that support the findings of this study are available from the corresponding author upon reasonable request.

ORCID

Atabak Azimi https://orcid.org/0009-0009-0606-5466
Stefan Koch https://orcid.org/0000-0003-4221-0834
Markus Reichhartinger https://orcid.org/0000-0003-4681-9575

REFERENCES

1. Zhang L, Deng T, Klemeš JJ, Zeng M, Ma T, Wang Q. Supercritical CO2 Brayton cycle at different heat source temperatures and its analysis under leakage and disturbance conditions. *Energy*. 2021;237:121610.
2. Sun Y, Zhang L, Peng Y, Chen Y, Lin Y. Response of a novel denitrifying phosphorus removal (AAO-BCO) system to sinusoidal flow perturbation of municipal sewage: adaptability, tolerance and improvement. *Sci Total Environ*. 2023;904:165837.
3. Xu Y, Mathelin dM, Knittel D. Adaptive rejection of quasi-periodic tension disturbances in the unwinding of a non-circular roll. *Proceedings of the 2002 American Control Conference (IEEE Cat. No. CH37301)*. Vol 5. IEEE; 2002:4009-4014.
4. Francis B, Wonham W. The internal model principle of control theory. *Automatica*. 1976;12(5):457-465. doi:10.1016/0005-1098(76)90006-6
5. Isidori A, Byrnes CI. Output regulation of nonlinear systems. *IEEE Trans Autom Control*. 1990;35(2):131-140.
6. Isidori A, Marconi L, Serrani A. *Robust Autonomous Guidance: An Internal Model Approach*. Springer Science & Business Media; 2003.
7. Marino R, Tomei P. Output regulation for linear systems via adaptive internal model. *IEEE Trans Autom Control*. 2003;48(12):2199-2202.
8. Obregon-Pulido G, Castillo-Toledo B, Loukianov AG. A globally adaptive internal model regulator for MIMO linear systems. *Proceedings of the 44th IEEE Conference on Decision and Control*. IEEE; 2005:4821-4826.
9. Zhang Z, Serrani A. Adaptive robust output regulation of uncertain linear periodic systems. *IEEE Trans Autom Control*. 2009;54(2):266-278.
10. Bin M, Bernard P, Marconi L. Approximate nonlinear regulation via identification-based adaptive internal models. *IEEE Trans Autom Control*. 2020;66(8):3534-3549.
11. Kim W, Kim H, Chung CC, Tomizuka M. Adaptive output regulation for the rejection of a periodic disturbance with an unknown frequency. *IEEE Trans Control Syst Technol*. 2010;19(5):1296-1304.
12. De Wit CC, Praly L. Adaptive eccentricity compensation. *IEEE Trans Control Syst Technol*. 2000;8(5):757-766.
13. Zhu Q. Complete model-free sliding mode control (CMFSMC). *Sci Rep*. 2021;11(1):22565.
14. Shtessel Y, Edwards C, Fridman L, Levant A. *Sliding Mode Control and Observation*. Vol 10. Springer; 2014.
15. Ebrahimi N, Ozgoli S, Ramezani A. Model-free sliding mode control, theory and application. *Proc Inst Mech Eng I J Syst Control Eng*. 2018;232(10):1292-1301.
16. Li P, Zhu G. Robust internal model control of servo motor based on sliding mode control approach. *ISA Trans*. 2019;93:199-208.
17. Zhang B, Nie K, Chen X, Mao Y. Development of sliding mode controller based on internal model controller for higher precision electro-optical tracking system. *Actuators*. Vol 11. MDPI; 2022:16.
18. Incremona GP, Mirkin L, Colaneri P. Integral sliding-mode control with internal model: a separation. *IEEE Control Syst Lett*. 2021;6:446-451.
19. Barth A, Reichhartinger M, Wulff K, Reger J, Koch S, Horn M. Indirect adaptive sliding-mode control using the certainty-equivalence principle. *Advances in Variable Structure Systems and Sliding Mode Control—Theory and Applications Springer International Publishing*. 2017:165-191. Springer.
20. Obregon-Pulido G, Castillo-Toledo B, Loukianov AG. A structurally stable globally adaptive internal model regulator for MIMO linear systems. *IEEE Trans Autom Control*. 2010;56(1):160-165.
21. Ficocelli M, Ben AF. Adaptive regulation of MIMO linear systems against unknown sinusoidal exogenous inputs. *Int J Adapt Control Signal Process*. 2009;23(6):581-603.
22. Marino R, Tomei P. Adaptive disturbance rejection for unknown stable linear systems. *Trans Inst Meas Control*. 2016;38(6):640-647.
23. Edwards C, Spurgeon S. *Sliding Mode Control: Theory and Applications*. CRC Press; 1998.
24. Hung JY, Gao W, Hung JC. Variable structure control: a survey. *IEEE Trans Ind Electron*. 1993;40(1):2-22.
25. Khalil HK. *Nonlinear Control*. Vol 406. Pearson New York; 2015.
26. Luenberger DG. *Dynamic Systems*. J. Wiley Sons; 1979.
27. Reichhartinger M, Falkensteiner R, Horn M. Robust estimation of forces for suspension system control. *IFAC-PapersOnLine*. 2018;51(25):328-333. doi:10.1016/j.ifacol.2018.11.128

How to cite this article: Azimi A, Koch S, Reichhartinger M. Robust internal model-based control for linear-time-invariant systems. *Int J Robust Nonlinear Control*. 2024;34(18):12476-12496. doi: 10.1002/rnc.7643

APPENDIX. PROOF OF LEMMA 1

The dynamic matrix in (10) has a special form and the stability of this unique matrix and the boundedness of the state $\mathbf{x}$ in (10) are investigated in the literature. The eigenvalues of the dynamic matrix consist of zero and roots of a polynomial which is Hurwitz because of the minimum phase assumption. The zero eigenvalue and its corresponding eigenvector are needed to analyze for the boundedness of $\mathbf{x}$ governed by system (10). Other eigenvalues enforce asymptotic stability due to their negative real parts. In this manner the equation for the left eigenvector of the dynamic matrix of the system (10) is

$$\begin{bmatrix} \rho_1^{\mathrm{T}} \\ \rho_2^{\mathrm{T}} \\ \vdots \\ \rho_n^{\mathrm{T}} \end{bmatrix} \left(\mathbf{I}_n - \frac{\mathbf{b}\mathbf{c}^{\mathrm{T}}}{\mathbf{c}^{\mathrm{T}}\mathbf{b}} \right) \mathbf{A} = \begin{bmatrix} 0 & 0 & 0 & \dots & 0 \\ 0 & \lambda_2 & 0 & \dots & 0 \\ 0 & 0 & \lambda_3 & \dots & 0 \\ \vdots & \vdots & \vdots & \ddots & \vdots \\ 0 & 0 & 0 & \dots & \lambda_n \end{bmatrix} \begin{bmatrix} \rho_1^{\mathrm{T}} \\ \rho_2^{\mathrm{T}} \\ \vdots \\ \rho_n^{\mathrm{T}} \end{bmatrix}, \tag{A1}$$

where ρ_i^{T} with $i = 1, \dots, n$ denoted the left eigenvector of dynamic matrix in (10) corresponding to the eigenvalues λ_{i} and $\lambda_1 = 0$. Besides, the eigenvector for the zero eigenvalue is

$$\begin{gathered} \rho_1^{\mathrm{T}} \left(\mathbf{I}_n - \frac{\mathbf{b}\mathbf{c}^{\mathrm{T}}}{\mathbf{c}^{\mathrm{T}}\mathbf{b}} \right) \mathbf{A} = \mathbf{0}_{1\times n} = \mathbf{c}^{\mathrm{T}} \left(\mathbf{I}_n - \frac{\mathbf{b}\mathbf{c}^{\mathrm{T}}}{\mathbf{c}^{\mathrm{T}}\mathbf{b}} \right) \mathbf{A}, \\ \rho_1^{\mathrm{T}} = \mathbf{c}^{\mathrm{T}}. \end{gathered} \tag{A2}$$

Therefore, the dynamic for the reduced order system for ρ_1^{T} can be computed by using (11)

$$\rho_1^{\mathrm{T}}\dot{\mathbf{x}} = \mathbf{c}^{\mathrm{T}}\dot{\mathbf{x}} = \dot{\sigma} - \mathbf{q}^{\mathrm{T}}\dot{\mathbf{w}}, \tag{A3}$$

The first part that is, $\dot{\sigma}$ vanished in a finite time based on the assumption in the Lemma 1. Equation (A3) with this consideration become

$$\rho_1^{\mathrm{T}}\dot{\mathbf{x}} = -\mathbf{q}^{\mathrm{T}}\dot{\mathbf{w}}, \tag{A4}$$

$$\rho_1^{\mathrm{T}}\mathbf{x} = -\mathbf{q}^{\mathrm{T}}\mathbf{w}. \tag{A5}$$

As long as disturbance $\mathbf{w}$ is bounded and $\mathbf{q}$ is constant, $\rho_1^{\mathrm{T}}\mathbf{x}$ is bounded.